Optics and Lasers in Engineering 50 (2012) 1242–1259

Contents lists available at SciVerse ScienceDirect

Optics and Lasers in Engineering

journal homepage: www.elsevier.com/locate/optlaseng

Best ellipse and cylinder parameters estimation from laser profile scan sections

Mohamed Rahayem [a,*], Naoufel Werghi [b], Johan Kjellander [a]

[a] Örebro University, Modeling and Simulation Research Center, Campus Alfred Nobel, Karlavägen 16, 691 41 Karlskoga, Sweden
[b] Khalifa University, Electrical and Computer Engineering Department, Sharjah Campus, Sharjah, United Arab Emirates

ARTICLE INFO

Article history:
Received 10 June 2011
Received in revised form
23 March 2012
Accepted 28 March 2012
Available online 14 April 2012

Keywords:
Ellipse fitting
Laser profile scanner
Industrial robot vision system
Pattern analysis
Curve fitting

ABSTRACT

Industrial applications like robot-aided welding, automated inspection, and 3D measurements require 3D points to be captured from the surfaces of objects and processed to calculate the information-of-interest. The lack of research focused on fitting ellipses to 3D laser profile data, and the intrinsic features that distinguish it from 2D digital images, motivated us to conduct a comparative study involving the most popular ellipse-fitting methods. After describing our laser profile scanning system, and a survey of ellipse-fitting methods, we compare, using extensive experiments performed with synthetic and real data, the fitting algorithms in terms of stability and accuracy with respect to a variety of factors. The estimate obtained with the best method is used to initialize a robust non-linear iterative ellipse fitting method. Finally, we describe a novel method for the construction of cylindrical surfaces from estimated elliptical sections.

1. Introduction

Point clouds are used in many applications, such as automatic inspection, Geometric Reverse Engineering (GRE), autonomous planning, and object recognition. In GRE applications, for example, point clouds are often processed using segmentation algorithm(s) that use geometrical reasoning to group homogeneous points into a single region. This region can be represented by specific shapes, like planes, cylinders, or other surfaces. Laser scanners are often used to rapidly acquire dense sets of 3D points from the surfaces of real-world objects. One example is a 3D laser scanning head that consists of a laser source and a digital camera mounted in a metal house with a well-defined angle between their axes. The scanner head setup, the calibration, and the integration with an industrial robot equipped with a turntable were presented in detail in [1–4]. Fig. 1 shows the scanner head mounted on an industrial robot arm.

The laser source projects a straight line onto the object surface, while the camera captures images of the line projection. The industrial robot controls the scanner movement along the planned scanning path and records the pose corresponding to each captured image. Fig. 2 shows how the scanner is mounted on the robot. The sequence of laser profiles generated while the robot moves along a path is registered in a common 3D coordinate system used by the robot and the turntable. This makes it possible to obtain "an organized point cloud".

In [5], we proposed a novel framework for GRE in which the region-growing segmentation procedure, unlike in previous approaches, does not operate on 3D point cloud data, but on structured 2D laser profiles called "chains" derived from their 3D laser counterparts. A chain is an ordered discrete set of points that encompass line and/or elliptic segments. We showed that to be fully effective this approach requires a consistent estimation of the ellipse parameters across different chains belonging to the same cylindrical surface; therefore, there is a need for a robust and reliable ellipse-fitting method.

Despite the fact that many ellipse-fitting algorithms have been developed for 2D applications, we did not find any reference to methods that process the elliptical section data captured by laser profile scanners. Elliptic curves in 2D images and chains are not issued from the same transformation pipeline. Furthermore, unlike in 2D image data, which might contain full or large sections of an ellipse, elliptic curves in laser profiles cannot exceed a half-ellipse portion. This limitation is intrinsic to the laser profile scanning technology. These considerations motivated us to investigate the best ellipse-fitting technique for our application.

In this paper, we propose an approach that blends two techniques, a robust linear estimation and a non-linear minimization. The robust linear estimation attempts to find the best initial estimate for the non-linear minimization to guarantee a convergence to a nearby solution.

* Corresponding author. Tel.: +46 19301137; fax: +46 58637318.
E-mail address: mohamed.rahayem@oru.se (M. Rahayem).

0143-8166/$ - see front matter © 2012 Elsevier Ltd. All rights reserved.
http://dx.doi.org/10.1016/j.optlaseng.2012.03.014

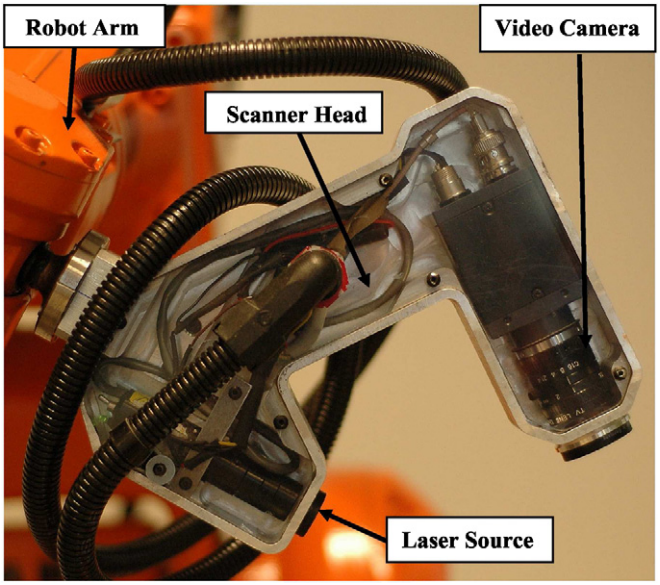

Fig. 1. The laser profile scanner components.

Fig. 2. The laser profile scanner mounted on an industrial robot equipped with a turntable.

The rest of the paper is organized as follows: Section 2 includes a comprehensive literature review covering laser profile scanners, as well as a brief description on how the profiles are obtained and processed in our system. Section 3 surveys the spectrum of ellipse-fitting methods. Section 4 describes in detail the methods selected for comparison and the non-linear iterative estimation method used for the final fitting. Section 5 describes how cylinders are created using ellipses. Section 6 is dedicated to experiments carried out on synthetic and real data. Section 7 discusses the experimental results. Finally, Section 8 concludes the paper and points out interesting directions for future work.

2. Laser profile scanners: a literature review

This section briefly reviews the most common laser profile scanners used in research and their industrial applications. Blais [6] reviewed 20 years of development in the field of 3D laser scanning, in which the author focused on commercial systems and compared them with each other. The author used the term "Slit Scanner" to describe the laser profile scanner. Pito and Bajcsy [7] presented a simple scanning system that combined a fixed range camera with a turntable to acquire a surface model, then solved the Next Best View (NBV) problem without prior knowledge of the part being measured. Two automated scanning systems were introduced by Chan et al. and Milroy et al. [8,9], respectively, where a Coordinate Measuring Machine (CMM) was used in combination with a laser profile scanner.

Feng et al., in [10,11], characterized and compensated for the digitizing errors of a 3D laser line scanner mounted on CMM with respect to scan depth and projected angle. Lee et al., in [12,13], used a laser profile scanner that consisted of two Charge-Coupled Device (CCD) cameras mounted on a three-axis transport mechanism. Son et al. [14] introduced a motorized rotary table with two Degrees of Freedom (DOF) and a laser profile scanner mounted on a Computer Numerical Control (CNC) machine with four DOFs to measure parts with free form surfaces.

Son et al. [15] presented a new method to scan complex surface models, using a stripe-type laser scanner that consisted of a laser source and two CCD cameras. The laser probe was mounted on a three-axis transportation mechanism. Xie et al. [16] presented a laser sensor, which consisted of three laser stripes and three CCD cameras, for measuring complex parts. The sensor was mounted on a CMM. Robertson and Fisher [17] showed how to use an orthogonal laser stripe scanner to extract models of screw-threads.

Callieri et al. [18] introduced the RobScan system. It is an automatic scanning system consisting of a commercial range laser scanner mounted on an industrial robot equipped with a turntable. This system uses a two-pass approach, whereby the second pass filled in the portions of the scanned model that were not visible in the first pass. The NBV algorithm was used to select viewpoints that maximized surface coverage with a minimum number of acquisitions, thus reducing the number of range maps. The system determines the poses of the scanner in space while registering the range maps in a reference frame. For more details on view planning and automated 3D object reconstruction and inspection, see [19]. Hayes et al. [20] presented an integrated optical-robotic measurement system, which was used to measure the external shape of cable connectors for manufacturing purposes. Reindl and O'Leary [21], O'Leary et al. [22], and Schalk and O'Leary [23] used a laser profile scanner to inspect peeled steel rods and to analyze the captured profiles of rotating objects, respectively. Bradley and Chan [24] used a 3D scanning system that employed a light-sectioning method to acquire shape features of biological objects.

A simple and low-cost 3D profile scanner was presented by Bradley et al. in [25]. Reinhart and Tekouo [26] presented an automatic programming algorithm, which was used by a robot-mounted laser line scanner for inspection tasks by automatically extracting features lines. The robot was equipped with a turntable and coupled with other robots. Van Gestel et al. [27] presented an

evaluation test of the performance of a laser profile scanner mounted on a CMM. D'Apuzzo [28] comprehensively reviewed different 3D surface digitizers being used in Europe. The survey included laser profile scanners that were mounted on CMMs and robots.

A fully automatic system, based on a laser profile scanner mounted on an industrial robot equipped with a turntable, was designed by Larsson and Kjellander [1–3]. The VARKON CAD tool [66] was used to model and simulate the scan paths and to store the captured data in a 3D triangular mesh. The mesh was segmented into regions, then surfaces were fitted to the segmented regions to create a final CAD model of the scanned object. The scan paths were generated automatically to scan unknown objects that might contain cylinders. This system was used to carry out the experiments presented in this paper (see Section 6). In this system, the object was scanned with an unknown angle between its surface normal and the scanner laser plane. As the scanner moves along a predefined scan path, the system outputs a sequence of profiles, F_i, where $i \in \{1,2,3,\ldots,M\}$ and M is the number of profiles. The profiles are stored in a queue data structure. Each of the 2D profiles obtained using this procedure consist of one or more chains, depending on occlusion and object geometry. Each chain is split into line and curve segments using the splitting algorithm developed by Rahayem and Kjellander [5]. Afterwards, a 3D region-growing procedure is performed to group line segments into planar regions and curve segments into quadratic regions.

3. Ellipse fitting: a survey

Ellipse fitting methods can be divided into three categories: clustering methods, linear least-square methods, and non-linear least-square methods.

3.1. Clustering methods – CMs

These methods, also known as voting methods, generally use Hough Transform (HT) [29,30], RANdom SAmple Consensus (RANSAC) [31], and Fuzzy Clustering (FC) techniques. They are robust against outliers, able to fit many curves simultaneously, and no pre-segmentation is required. Unfortunately, CM methods are computationally expensive, use a large amount of memory, and have relatively low accuracy. Some variants attempt, however, to address these shortcomings. Fei et al. [32] presented a novel ellipse detector that was used to process digital images. The new detector reduced computational cost and storage requirements by dividing an edge image into sub-images. Chia et al. [33] presented a novel ellipse detection algorithm that minimized the storage and computational complexity by using a one-dimensional accumulator. The algorithm was parallelized to improve the speed of computation. Despite these improvements, these methods are still not suited to real-time applications.

3.2. Least-square methods – LSMs

LSMs are based on the minimization of an energy function that represents the sum of Euclidean distances between N points and the ellipse being fitted

$$E(\vec{a}) = \sum_{i=1}^{N} d(\vec{a},\vec{x_i}) \tag{1}$$

where $\vec{a} = [a,b,c,d,e,f]^T$ is the parameters vector of the conic section, $\vec{x_i} = [x_i^2, x_i y_i, y_i^2, x_i, y_i, 1]$ is the data point vector, $d(\vec{a},\vec{x_i})$ is the distance function, and $E(\vec{a})$ is the energy function. LSMs are faster and more accurate than CMs, but are sensitive to outliers, and are only able to fit one ellipse at a time. The algebraic distance is used as an approximation of the Euclidean distance because it can be expressed as a simple linear equation, which is subsequently solved using appropriate non-iterative methods. The algebraic distance is defined by the following scalar product:

$$F(\vec{x_i}) = \vec{x_i} \cdot \vec{a} \tag{2}$$

The minimization of the sum-of-squared algebraic distances between the measurement points and the fitted conic is given by:

$$\min \sum_{i=1}^{N} F(\vec{x_i})^2 \tag{3}$$

Ordinary Least-square Ellipse Fitting (OLSEF), presented by Gander et al. [34], is a typical example of an LSM, where $\|\vec{a}\| = 1$. These methods are non-invariant for Euclidean coordinate transformation.

Methods based on a linearization of the Euclidean distance are called Linear Least-square Methods (LLSMs). Bookstein, in [35], used a specific constraint to fit conic sections, including ellipses, to scattered data; we call this method Bookstein Constrained Ellipse Fitting (BCEF). Gander et al. [34] presented a trace constraint to fit an ellipse and hyperbola, a method we call Trace Constrained Ellipse Fitting (TCEF). A nice introduction of these techniques is given by Zhang [36]. A simple LLSM was used by Jianfei et al. [37] to detect ellipses in images of complex environments. Wan and Ventura [38] used a simple LLSM algorithm to segment straight lines and elliptical arcs of boundary contours for machined parts. O'Leary and Zsombor-Murry [39] introduced a method based on quadratic constraint for specific hyperbola and ellipse fitting. A later version presented by O'Leary et al. [40] was extended to fit coupled geometric objects, such as concentric circle and ellipses. A reliable linearization of Euclidean distances based on Taylor's series is published by Taubin [41]; we call this method Taubin Linear-approximation Ellipse Fitting (TLAEF).

Harker et al. [42] presented a new linear method, which is used to perform direct fitting of scattered point data specifically to ellipses and hyperbolae with eigenvalue bias correction. In addition, a linear method of correcting the bias of a linear conic fit was presented. Hahn et al. [43] proposed a new algorithm for ellipse detection using curve segments in an edge image. Fitzgibbon et al. [44] presented a novel and robust algorithm called Direct Ellipse-Specific Fitting (DESF), which was constrained to the fitting of an ellipse, rather than a general conic section.

Wu [45] used the DESF algorithm to develop a robust real-time algorithm that automatically and accurately detects and locates ellipses in digital images. Halir\widehat and Flusser [46] improved the DESF algorithm and increased its numerical stability, which we refer to as Improved Specific Ellipse Fitting (ISEF). Nguyen et al. [47] developed a real-time ellipse detection algorithm based-on the ISEF. Maini [48] enhanced DESF by re-centering and scaling the data to reduce the ill-conditioning of the scatter matrix. The DESF algorithm fails in practice when noiseless, or even low noise, data is being used. Maini eliminated this failure by adding noise with a known distribution and repeating the fitting times, using an algorithm known as Enhanced Direct Least-squares Fitting of Ellipses (EDFE).

Schleicher and Zagar [49] modified DESF by introducing boundary conditions to fit concentric ellipses in order to measure the ellipticity of steel coil using a vision system. Greggio et al. [50] presented a new algorithm that eliminated the numerical instability of DESF and performed better than EDFE when noiseless data was used. Barwick [51] presented a real-time least-squares method for iris and pupil segmentation in eye images. The method presented employed an indirect geometric fit based on the quadratic polynomial of parallel chord lengths. The algorithm was computationally efficient and robust to outliers,

but the technique as a whole was too specific to eye images applications.

Another category of methods use different variants of Kalman filtering, using the algebraic distance [52,53] or an approximation of the Euclidean distance [54,55] to localize objects from 2D images based on circular patterns. Werghi et al. [55] proposed a linearization of the Euclidean distance error, by which the ellipse parameters could be estimated using an Extended Kalman Filter Ellipse Fitting (EKFEF).

3.3. Non-Linear Least-square Methods – NLSMs

NLSMs are the most accurate ellipse-fitting methods, sometimes also referred to as Best ellipse fitting, Geometric ellipse fitting, Euclidean ellipse fitting, Orthogonal-distance ellipse fitting, or Parametric ellipse fitting.

In general, a nonlinear algorithm first requires an initial estimate for the parameters, which can be calculated by algebraic or approximate geometric fitting. Second, it requires an iterative or non-linear optimization algorithm, such as the Gauss–Newton (GN) or Levenberg–Marquardt (LM) algorithms, to minimize the objective function, which is the distance equation between the measured points and the ellipse. Finally, a stop criteria must be met in the case of convergence. In practice, LM is preferable where the data points may fit a circle, i.e. the semi-major and semi-minor axes of the fitted ellipse are equal or very close to being equal. The GN method fails if the Jacobian becomes a singular matrix.

Ahn et al. [56,57] used LM to fit ellipses, circles, hyperbolas, and parabolas. Gander et al. [34] used GN and LM techniques to fit circles and ellipses to a set of points. A very detailed study published by Faber and Fisher [58] compared the performance of fitting algorithms in terms of efficiency, correctness, robustness, and pose invariance.

4. Ellipse-fitting methods

4.1. Non-iterative ellipse fitting

In the following, we will describe the six standard ellipse fitting methods that are compared in Section 6.

1. *Ordinary Least-square Ellipse Fitting* (OLSEF).
   OLSEF is the most common method of those that use the algebraic distances minimization. The method is straightforward and starts by creating a $n \times 6$ design matrix $\mathbf{D}$ from the data points, as follows:

$$\mathbf{D} = \begin{bmatrix} x_1^2 & x_1 \cdot y_1 & y_1^2 & x_1 & y_1 & 1 \\ \vdots & \vdots & \vdots & \vdots & \vdots & \vdots \\ x_n^2 & x_n \cdot y_n & y_n^2 & x_n & y_n & 1 \end{bmatrix} \tag{4}$$

   Using Singular Value Decomposition (SVD), $\mathbf{D}$ is decomposed into three matrices:

$$\mathbf{D} = \mathbf{U} \cdot \mathbf{W} \cdot \mathbf{V}^T \tag{5}$$

   The solution vector $\vec{a}$ is equal to the sixth normalized column of the matrix $\mathbf{V}$:

$$\vec{a} = \mathbf{V}(i,6), \quad i = 1, \ldots, 6. \tag{6}$$

   $\mathbf{D}$ can become ill-conditioned or even singular. It is recommended to use mean-free data and SVD decomposition rather than other decomposition techniques, such as eigenvalue decomposition. Refer to [34] for more details.

2. *Improved Specific Ellipse Fitting* (ISEF).
   In this method, $\mathbf{D}$, as given by Eq. (4), is decomposed into a quadric and linear sub-matrices $\mathbf{D}_1$ and $\mathbf{D}_2$:

$$\mathbf{D} = [\mathbf{D}_1 | \mathbf{D}_2] \tag{7}$$

   where

$$\mathbf{D}_1 = \begin{bmatrix} x_1^2 & x_1 \cdot y_1 & y_1^2 \\ \vdots & \vdots & \vdots \\ x_n^2 & x_n \cdot y_n & y_n^2 \end{bmatrix}$$

   and

$$\mathbf{D}_2 = \begin{bmatrix} x_1 & y_1 & 1 \\ \vdots & \vdots & \vdots \\ x_n & y_n & 1 \end{bmatrix}$$

   A new scatter matrix $\mathbf{S}$ is formulated as follows:

$$\mathbf{S} = \begin{bmatrix} \mathbf{S}_1 & \mathbf{S}_2 \\ \mathbf{S}_2^T & \mathbf{S}_3 \end{bmatrix} \tag{8}$$

   where $\mathbf{S}_1 = \mathbf{D}_1^T \mathbf{D}_1$, $\mathbf{S}_2 = \mathbf{D}_1^T \mathbf{D}_2$, and $\mathbf{S}_3 = \mathbf{D}_2^T \mathbf{D}_2$.
   The ellipse constraint matrix $\mathbf{C}$ of size 3×3 is defined as

$$\mathbf{C} = \begin{bmatrix} 0 & 0 & 2 \\ 0 & -1 & 0 \\ 2 & 0 & 0 \end{bmatrix} \tag{9}$$

   The coefficients vector $\vec{a}$ is split into $\vec{a_1}$ and $\vec{a_2}$:

$$\vec{a} = \begin{bmatrix} \vec{a_1} \\ --- \\ \vec{a_2} \end{bmatrix} \tag{10}$$

   where $\vec{a_1} = [a,b,c]^T$ and $\vec{a_2} = [d,e,f]^T$.
   The solution procedure is described by the following equations:

$$\mathbf{S}_1 \vec{a_1} + \mathbf{S}_2 \vec{a_2} = \lambda \mathbf{C} \vec{a_1} \tag{11}$$

$$\mathbf{S}_2^T \vec{a_1} + \mathbf{S}_3 \vec{a_2} = 0 \tag{12}$$

   Re-arranging Eq. (12), $\vec{a_2}$ gives

$$\vec{a_2} = -\mathbf{S}_3^{-1} \mathbf{S}_2^T \vec{a_1} \tag{13}$$

   Substitution of Eq. (13) into Eq. (11) yields

$$(\mathbf{S}_1 - \mathbf{S}_2 \mathbf{S}_3^{-1} \mathbf{S}_2^T) \vec{a_1} = \lambda \mathbf{C} \vec{a_1} \tag{14}$$

   Because $\mathbf{C}$ is a regular matrix, multiplication with $\mathbf{C}^{-1}$ gives

$$\mathbf{C}^{-1} (\mathbf{S}_1 - \mathbf{S}_2 \mathbf{S}_3^{-1} \mathbf{S}_2^T) \vec{a_1} = \lambda \vec{a_1} \tag{15}$$

   Use eigenvalue decomposition to decompose asymmetric reduced scatter matrix $\mathbf{M}$, where $\mathbf{M}$ is a 3×3 matrix given by:

$$\mathbf{M} = \mathbf{C}^{-1} (\mathbf{S}_1 - \mathbf{S}_2 \mathbf{S}_3^{-1} \mathbf{S}_2^T) \tag{16}$$

   The eigenvector that corresponds to the smallest non-negative eigenvalue λ_{min} is the solution of $\vec{a_1}$

$$\mathbf{M} \vec{a_1} = \lambda \vec{a_1} \tag{17}$$

   Finally, calculate $\vec{a_2}$ from Eq. (13). This method was published by Halir\widehat and Flusser [46].

3. *Taubin Linear-approximation Ellipse Fitting* (TLAEF).
TLAEF involves fitting an ellipse using a design matrix **Q**, such as in OLSEF. This method is an alternative to minimizing the linear distance in LLSM and uses an approximation of the Euclidean distance by expanding Eq. (1) with Taylor's series. The first order approximation of Eq. (1) is

$$\frac{f(\vec{x},\vec{a})}{\|\nabla f(\vec{x},\vec{a})\|} \tag{18}$$

Furthermore, Taubin adopts the following approximation of the Energy function:

$$\sum_i \frac{f(\vec{x},\vec{a})}{\|\nabla f(\vec{x},\vec{a})\|} = \frac{\sum_i f(\vec{x},\vec{a})}{\sum_i \|\nabla f(\vec{x},\vec{a})\|} \tag{19}$$

Statistically, the above approximation does not guarantee optimal estimates, but it allows a closed-form solution by eigenvalue decomposition:

$$\mathbf{Q}\cdot\vec{a} = \lambda\cdot\mathbf{DQ}.\vec{a} \tag{20}$$

where $\mathbf{Q} = (1/N)\sum_{i=1}^{N} q_i\cdot q_i^T$ and $\mathbf{DQ} = (1/N)\sum_{i=1}^{N} dq_i\cdot dq_i^T$ are the symmetric matrices, and where $q_i = [x_i^2, x_i\cdot y_i, y_i^2, x_i, y_i, 1]^T$ and dq_i is the Jacobian matrix of q_i with respect to x and y. The coefficients vector is equal to the eigenvector corresponding to the smallest eigenvalue given by Eq. (20). Among linear non-iterative ellipse-fitting methods, this approximation is perhaps the most accurate and robust; however, for a small number of data points it can return a conic that is not an ellipse.

4. *Bookstein Constrained Ellipse Fitting* (BCEF).
Fit an ellipse by using the $n\times 6$ design matrix **B**:

$$\mathbf{B} = \begin{bmatrix} x_1 & y_1 & 1 & x_1^2 & \sqrt{2}\cdot x_1\cdot y_1 & y_1^2 \\ \vdots & \vdots & \vdots & \vdots & \vdots & \vdots \\ x_n & y_n & 1 & x_n^2 & \sqrt{2}\cdot x_n\cdot y_n & y_n^2 \end{bmatrix} \tag{21}$$

and solve for the coefficient vector $\vec{a}$:

$$\vec{a} = [a, 2b, c, d, e, f]^T \tag{22}$$

With the constraint $\|\vec{a}\| = 1$, two vectors are defined: $\vec{v} = [d, e, f]^T$, $\vec{w} = [a, \sqrt{2}b, c]^T$.
The Bookstein constraint is written as $\|\vec{w}\| = 1$. The system to solve is

$$\mathbf{B}\cdot\begin{bmatrix}\vec{v}\\ \vec{w}\end{bmatrix} \approx 0 \tag{23}$$

Decompose the matrix **B** by QR decomposition and formulate the system:

$$\begin{bmatrix}\mathbf{R_{11}} & \mathbf{R_{12}}\\ 0 & \mathbf{R_{22}}\end{bmatrix}\cdot\begin{bmatrix}\vec{v}\\ \vec{w}\end{bmatrix} \approx 0 \tag{24}$$

This system can be solved as the following:

$$\mathbf{R_{22}}\cdot\vec{w} \approx 0, \quad \|\vec{w}\| = 1 \tag{25}$$

Decompose the matrix R_{22} into **U S** $\mathbf{H}^T$ matrices by SVD decomposition to find $\vec{w} = \mathbf{H}(i,3)$, $i = 1,2,3$, and then:

$$\vec{v} = \mathbf{R_{11}^{-1}}\cdot\mathbf{R_{12}}\cdot\vec{w} \tag{26}$$

This method was published by Bookstein [35].

5. *Trace Constrained Ellipse Fitting* (TCEF).
Fits an ellipse by solving the following system of equations:

$$\begin{bmatrix} 2x_1y_1 & x_1^2-y_1^2 & x_1 & y_1 & 1 \\ \vdots & \vdots & \vdots & \vdots & \vdots \\ 2x_ny_n & x_n^2-y_n^2 & x_n & y_n & 1 \end{bmatrix}\vec{v} \approx \begin{bmatrix} -x_1^2 \\ \vdots \\ -x_n^2 \end{bmatrix} \tag{27}$$

The above system can be solved by any numerical method, such as pseudo-inverse or Gauss elimination. The coefficients vector is

$$\vec{a} = [1-\vec{v}(2), \vec{v}]^T \tag{28}$$

This method was introduced by Gander et al. [59].

6. *Extended Kalman Filter Ellipse Fitting* (EKFEF).
This method, proposed by Werghi et al. [55], adopted a fitting error criterion based on the Maximum Likelihood (ML) estimation of both the parameter vector $\vec{a}$ and the orthogonal distance between the measurement point and the fitted ellipse. It also reduces the parameter vector $\vec{a}$ to $[a,b,d,e,f]^T$, using the normalization $a+c=1$, and the measurement vector to $\vec{x} = [x^2-y^2, xy, x, y, 1]$. The error criterion is defined as follows:

$$J = (\vec{a}-\hat{a})^T\mathbf{S}^{-1}(\vec{a}-\hat{a}) + \sum_{i=1}^{n}\frac{1}{R_i^2}(z_i - h_i^T\vec{a})^2 \tag{29}$$

The first and the second terms correspond to the ML of, respectively, $\vec{a}$ and an approximation of the orthogonal distance, where

$$R^2 = \frac{\partial F}{\partial\vec{x}}^T\mathbf{L}^{-1}\frac{\partial F}{\partial\vec{x}} \tag{30}$$

$$h = \frac{\partial F}{\partial\vec{a}} - \frac{1}{R^2}\frac{\partial R}{\partial\vec{a}} \tag{31}$$

$$z = -F(\vec{a},Y) + h^T\vec{a} \tag{32}$$

S and **L** are the covariance matrices of $\vec{a}$ and the gradient $\partial F/\partial\vec{x}$, respectively. Using the above linearization, the parameter vector $\vec{a}$ minimizing Eq. (29) is determined using the recursive Kalman filter equations:

$$K_i = S_{i-1}h(R^2 + h^T S_{i-1}h)^{-1} \tag{33}$$

$$\vec{a_i} = \overrightarrow{a_{i-1}} + K_i(z_i - h^T\overrightarrow{a_{i-1}}) \tag{34}$$

$$S_i = S_{i-1} - K_i h^T S_{i-1} \tag{35}$$

4.2. Iterative ellipse fitting

In the previous section, linear methods were used to find the initial estimates of the ellipse. An experimental comparison between them was carried out and explained in Section 6. In order to find the most accurate ellipse parameters' values, a non-linear "Iterative" method presented by Gander et al. [34], which involves the LM optimization technique, is used. We called this method Best Ellipse Fitting (BEF).

The ellipse can be represented in a parametric form using five parameters $\langle x_c, y_c, a, b, \phi\rangle$, where x_c, y_c are the ellipse center coordinates, a,b are the semi-major and semi-minor axes, and ϕ is the rotation angle between the semi-major axis and x-axis, respectively. Therefore, any point on an ellipse can be given by the equation

$$\begin{bmatrix} x_i \\ y_i \end{bmatrix} = \begin{bmatrix} x_c \\ y_c \end{bmatrix} + \mathbf{R}(\phi)\cdot\begin{bmatrix} a\cdot\cos(\alpha_i) \\ b\cdot\sin(\alpha_i) \end{bmatrix} \tag{36}$$

where $\mathbf{R}(\phi)=\left[\begin{smallmatrix}\cos(\phi) & -\sin(\phi)\\ \sin(\phi) & \cos(\phi)\end{smallmatrix}\right]$ and α is the angle between one end of the semi-major axis and the point ith counted from the center of the ellipse. We are then iterating to achieve an optimal result:

$$\begin{bmatrix} x_i \\ y_i \end{bmatrix} - \begin{bmatrix} x_c \\ y_c \end{bmatrix} + \mathbf{R}(\phi) \cdot \begin{bmatrix} a \cdot \cos(\alpha) \\ b \cdot \sin(\alpha) \end{bmatrix} \approx 0 \tag{37}$$

For $i=1,\ldots,n$, we have $2\times n$ nonlinear equations for $n+5$ unknowns $\langle x_c,y_c,a,b,\phi,\alpha_1,\ldots,\alpha_n,\rangle$. A Jacobian matrix is established by computing the partial derivatives of Eq. (37) with respect to all unknowns

$$\mathbf{J}=\begin{bmatrix} -a\cdot\mathbf{A} & \mathbf{C} \\ b\cdot\mathbf{B} & \mathbf{D} \end{bmatrix} \tag{38}$$

where $\mathbf{A}$ and $\mathbf{B}$ are the two $n\times n$ diagonal matrices $\mathbf{A}=$ diag $(\sin\alpha_i)$ and $\mathbf{B}=\text{diag}(\cos\alpha_i)$. $\mathbf{C}$ and $\mathbf{D}$ are $n\times 5$ and given as

$$\mathbf{C}=\begin{bmatrix} -b\cdot\sin(\alpha_1) & \cos(\alpha_1) & 0 & \cos(\phi) & \sin(\phi) \\ \vdots & \vdots & \vdots & \vdots & \vdots \\ -b\cdot\sin(\alpha_n) & \cos(\alpha_n) & 0 & \cos(\phi) & \sin(\phi) \end{bmatrix} \tag{39}$$

$$\mathbf{D}=\begin{bmatrix} a\cdot\cos(\alpha_1) & 0 & \sin(\alpha_1) & -\sin(\phi) & \cos(\phi) \\ \vdots & \vdots & \vdots & \vdots & \vdots \\ a\cdot\cos(\alpha_n) & 0 & \sin(\alpha_n) & -\sin(\phi) & \cos(\phi) \end{bmatrix} \tag{40}$$

Finally, the iterative and non-iterative methods are implemented in MATLAB [60]. The code is available upon request from the authors.

5. Application to cylindrical surface construction

In this paper, a geometric fitting approach for an ellipse is used to calculate the initial estimates of cylinder surfaces fitting. This method is based on the linear relationship between the radius of the circular section of the ellipse and the minor radius of the elliptical section of a right cylinder, as illustrated in Fig. 3. In other words, the circular section of the cylinder can be represented by a circle with a radius b and a center O. From descriptive geometry we have the following relationships:

$$\overline{OF_1}=\overline{OF_2}=c$$

$$a^2=b^2+c^2$$

$$\cos\phi=b/a \tag{41}$$

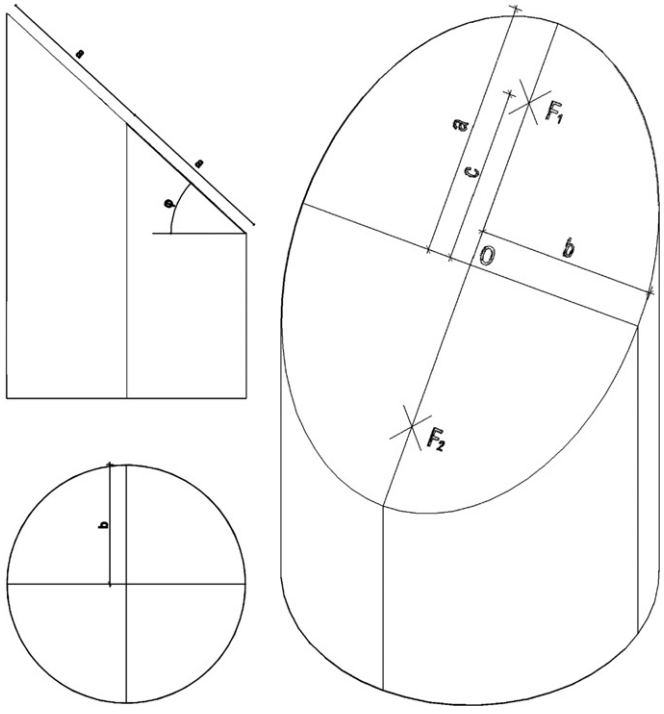

Fig. 3. The elliptical section of the cylinder.

5.1. Initial estimates

The fitted cylinder is defined by:

- A point (x_p,y_p,z_p) on its axis.
- A vector $[a,b,c]$ pointing along the axis direction.
- A radius r.

In most cylinder fitting methods, the initial estimates (x_p,y_p,z_p), $[a,b,c]$, and r are calculated by fitting a general quadric surface using LSM

$$\vec{x}\,\mathbf{P}\,\vec{x}^{\,T}+\vec{q}\,\vec{x}^{\,T}+J=0 \tag{42}$$

where $\mathbf{P}$ is a 3×3 matrix, $\vec{q}$ is a 1×3 row vector, and J is a scalar. The coefficients of quadric surface are used to calculate the initial estimates, see Werghi et al. [62]. With this method, at least nine points are required to solve Eq. (42), otherwise, it is not clear what can be done, as the number of points is less than the number of unknowns (see [63]).

In our method, the initial parameters are calculated using ellipses from three consecutive profiles, as follows:

- A 3D line is fitted to the ellipse centers in order to evaluate the cylinder axis direction vector.
- A point on the fitted line corresponds to a point on the cylinder axis.
- The cylinder radius is equal to the average of the semi-minor axes of the fitted ellipses.

These estimates are used by the algorithm in Section 5.2 to fit the best cylinder using a non-linear method.

The method presented is fast and suitable for real-time applications because it uses a few 2D points, rather than numerous 3D points. The method was originally described in a thesis by one of the authors (see [61]). This data reduction increases the speed of computation and reduces memory usage. See Section 6 for experimental results.

5.2. Best cylinder fitting

Assume a set of N points (x_i,y_i,z_i), where $i=1,\ldots,N$ and $N\geq 7$ belong to a cylindrical region. A distance from a point (x_i,y_i,z_i) to the cylinder is calculated by

$$d_i=r_i-r \tag{43}$$

where

$$r_i=\frac{\sqrt{[u_i^2+v_i^2+w_i^2]}}{\sqrt{[a^2+b^2+c^2]}} \tag{44}$$

and

$$u_i=c(y_i-y_p)-b(z_i-z_p) \tag{45}$$

$$v_i=c(z_i-z_p)-c(x_i-x_p) \tag{46}$$

$$w_i=c(x_i-x_p)-a(y_i-y_p) \tag{47}$$

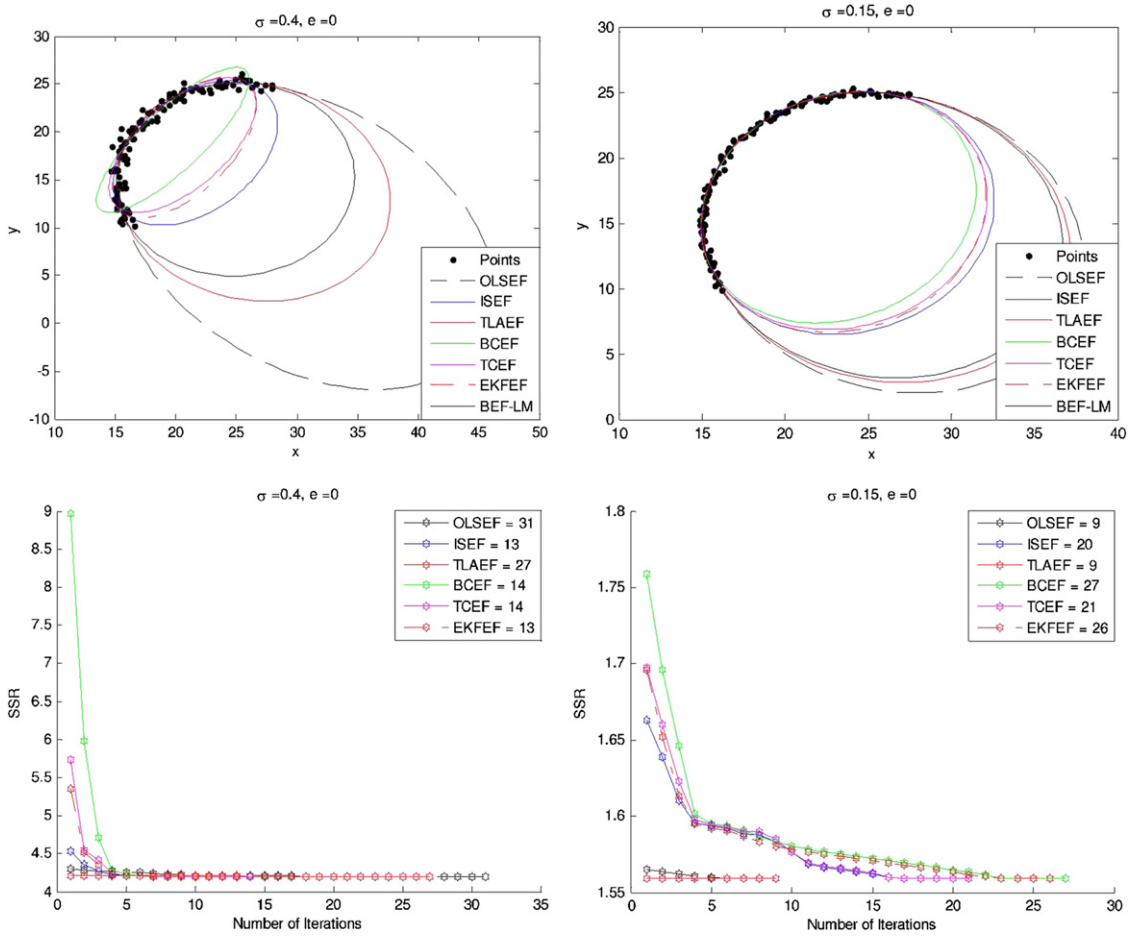

Fig. 4. Noise amplitudes (0.4 and 0.15), eccentricity (0), and the low-curvature arc.

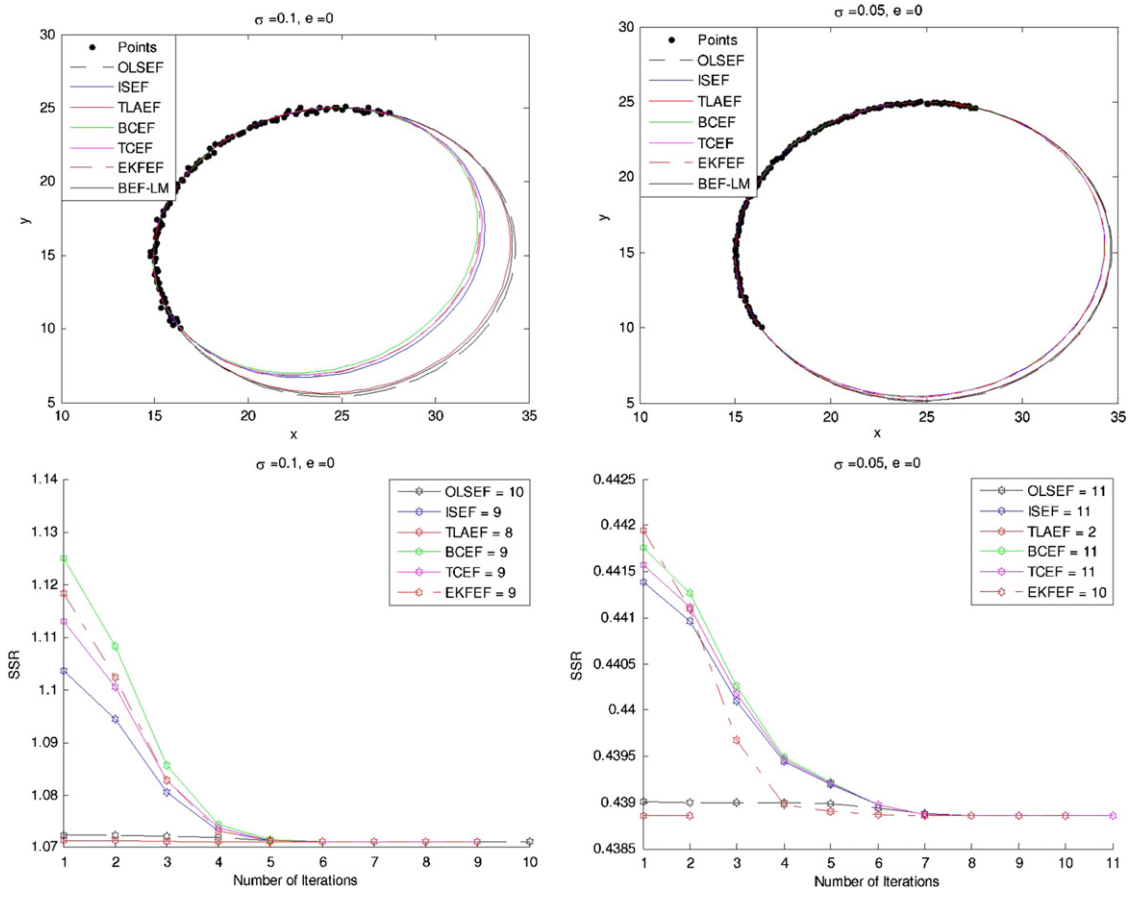

Fig. 5. Noise amplitudes (0.1 and 0.05), eccentricity (0), and the low-curvature arc.

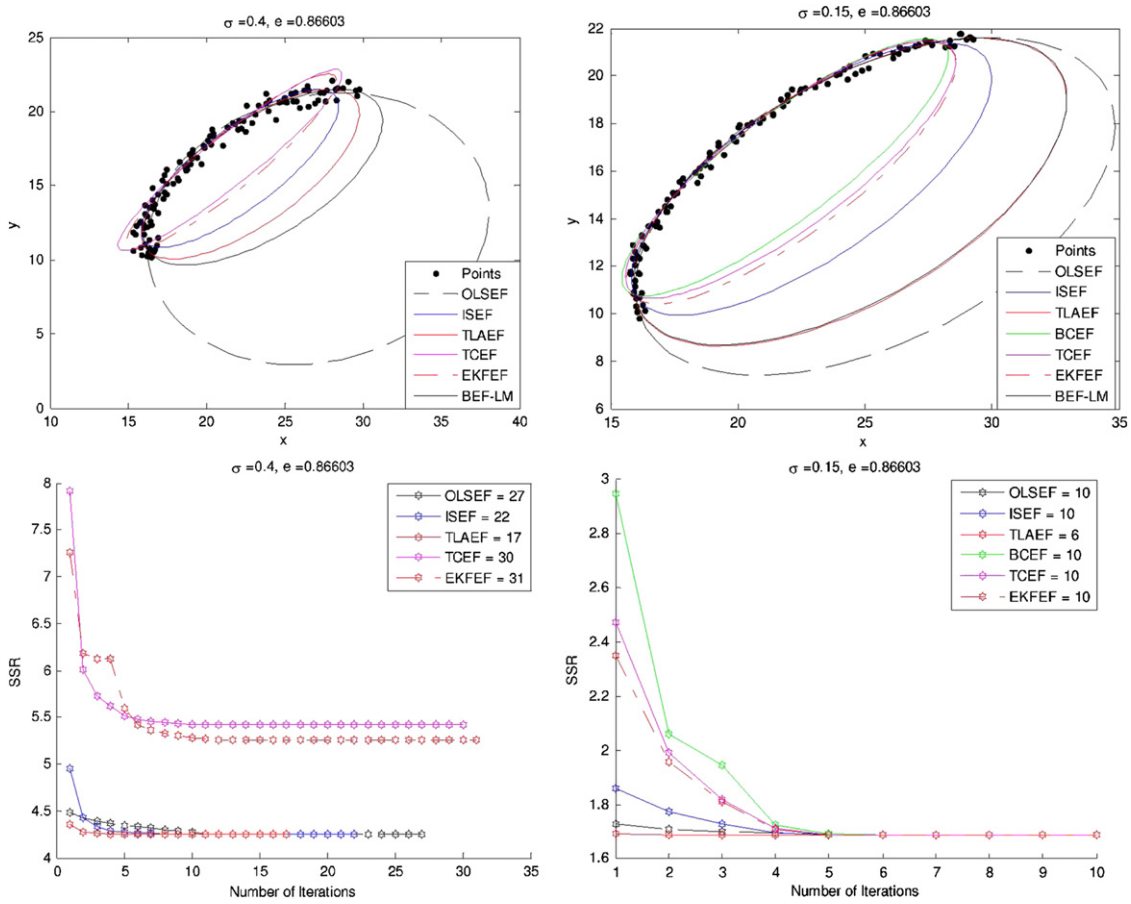

Fig. 6. Noise amplitudes (0.4 and 0.15), eccentricity (0.866), and the low-curvature arc.

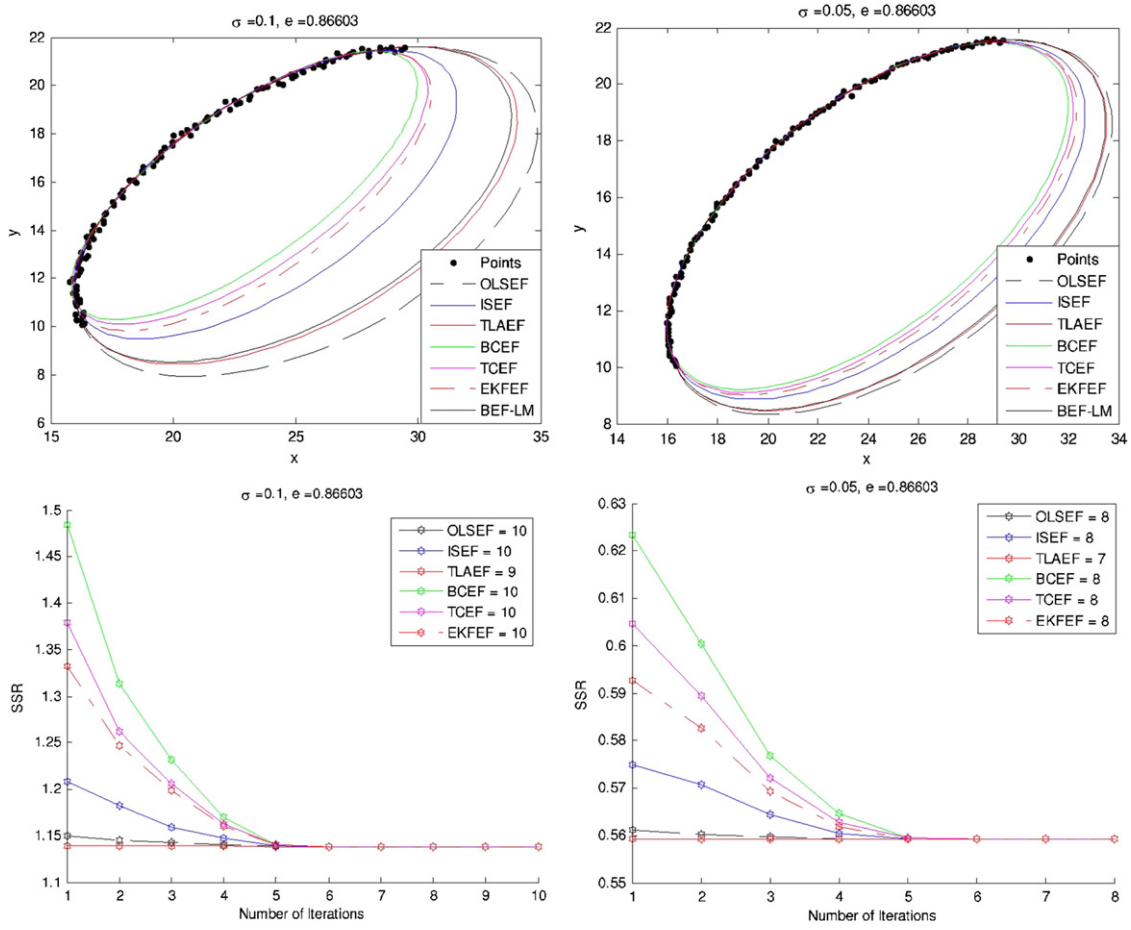

Fig. 7. Noise amplitudes (0.1 and 0.05), eccentricity (0.866), and the low-curvature arc.

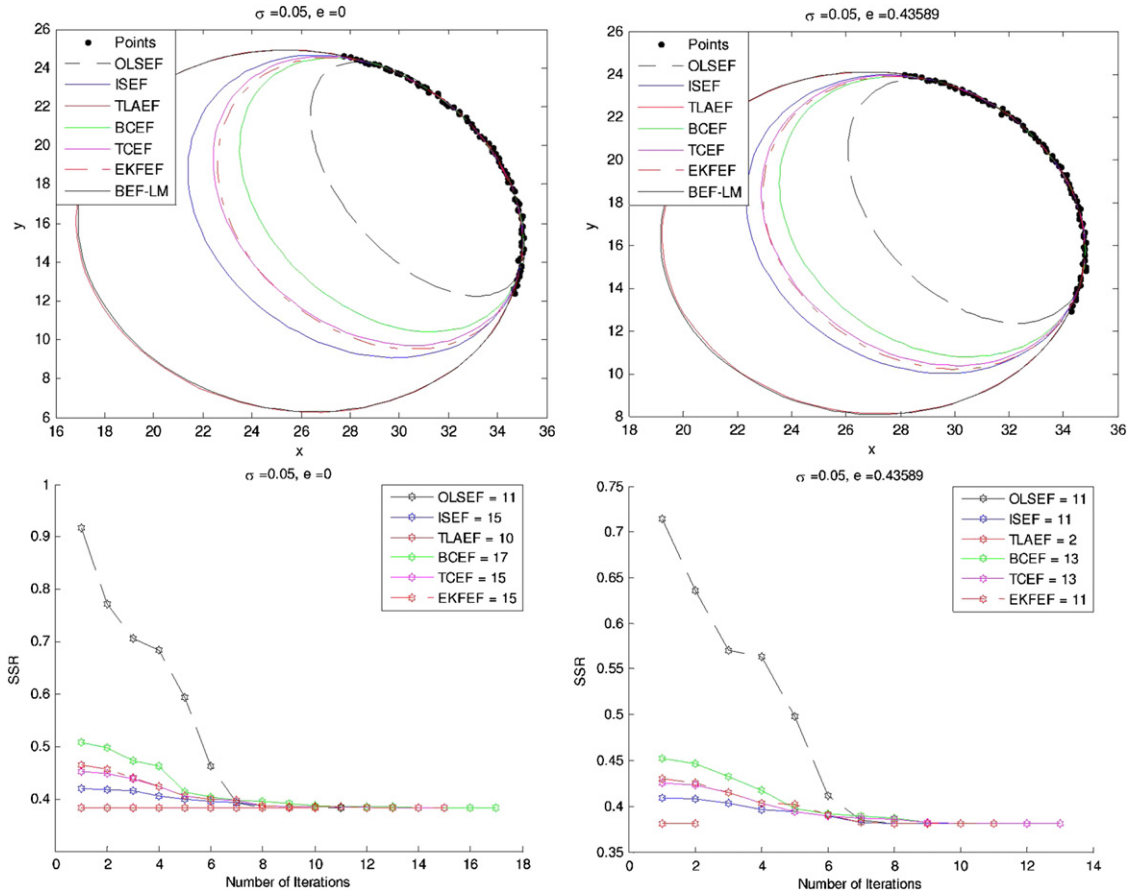

Fig. 8. Noise amplitude (0.05), eccentricity (0 and 0.435), and the high-curvature arc.

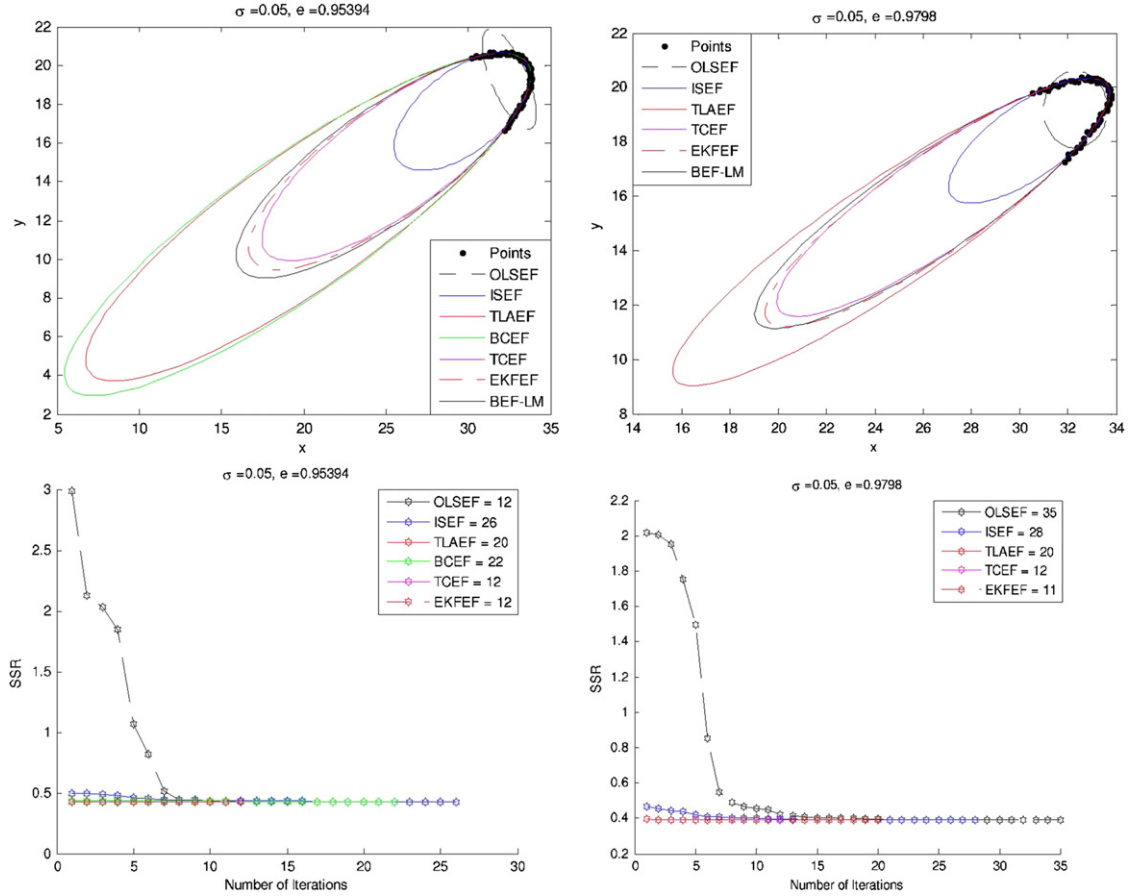

Fig. 9. Noise amplitude (0.05), eccentricity (0.954 and 0.979), and the high-curvature arc.

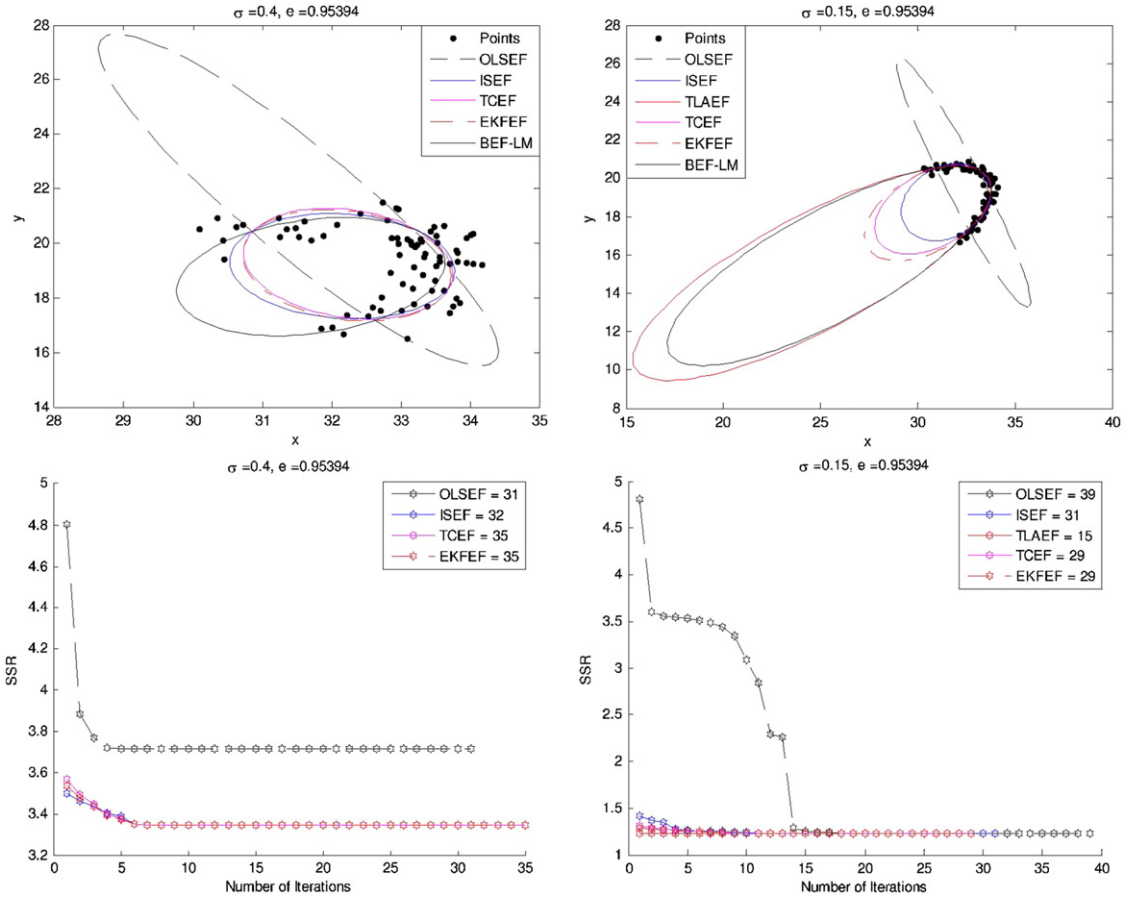

Fig. 10. Noise amplitudes (0.4 and 0.15), eccentricity (0.954), and the high-curvature arc.

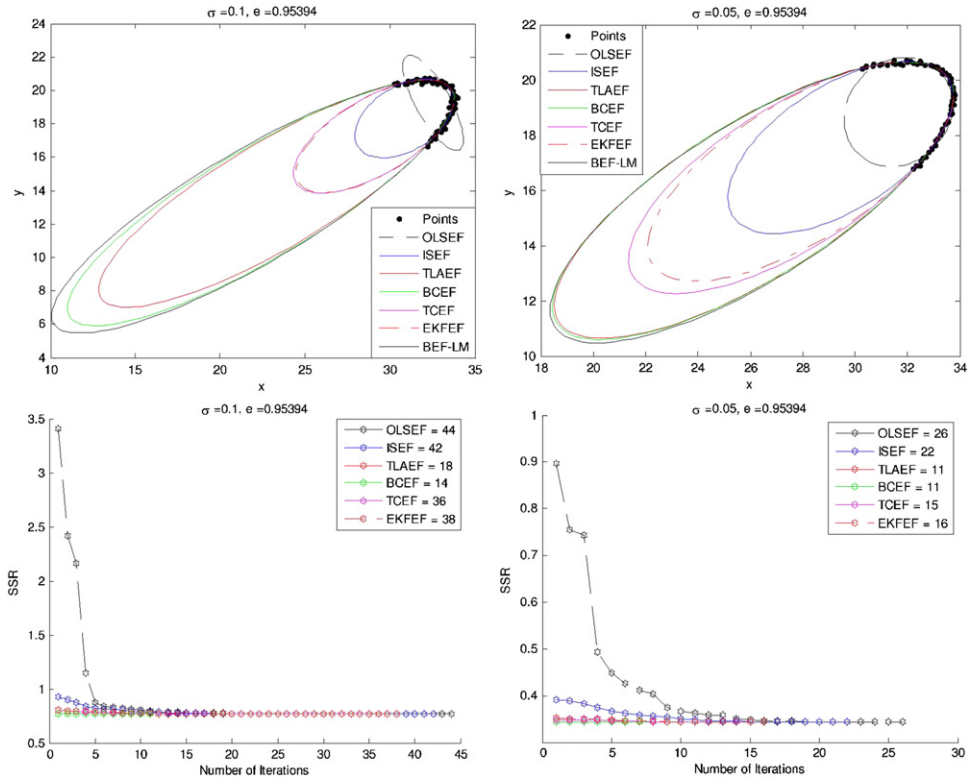

Fig. 11. Noise amplitudes (0.1 and 0.05), eccentricity (0.954), and the high-curvature arc.

and

$$r_i = \sqrt{(x_i^2 + y_i^2 + z_i^2)} \tag{48}$$

where r_i is the distance between the point ith and the cylinder axis. It is clear that (u_i, v_i, w_i) is the cross product of the vector $[(x_i, y_i, z_i) - (x_p, y_p, z_p)]$ with vector $[a, b, c]$.

The LM is used to minimize the sum of squares of the distances calculated by Eq. (43).

The Jacobian matrix is formulated by calculating the partial derivative of Eq. (43) as follows:

$$\mathbf{J} = \begin{bmatrix} \frac{\partial d_i}{\partial x_p} & \frac{\partial d_i}{\partial y_p} & \frac{\partial d_i}{\partial z_p} & \frac{\partial d_i}{\partial a} & \frac{\partial d_i}{\partial b} & \frac{\partial d_i}{\partial c} & \frac{\partial d_i}{\partial r} \\ \vdots & \vdots & \vdots & \vdots & \vdots & \vdots & \vdots \\ \frac{\partial d_n}{\partial x_p} & \frac{\partial d_n}{\partial y_p} & \frac{\partial d_n}{\partial z_p} & \frac{\partial d_n}{\partial a} & \frac{\partial d_n}{\partial b} & \frac{\partial d_n}{\partial c} & \frac{\partial d_n}{\partial r} \end{bmatrix}$$

where

- $\partial d_i/\partial x_p = -x_i/r_i$
- $\partial d_i/\partial y_p = -y_i/r_i$
- $\partial d_i/\partial z_p = -z_i/r_i$
- $\partial d_i/\partial a = -x_i z_i/r_i$
- $\partial d_i/\partial b = -y_i z_i/r_i$
- $\partial d_i/\partial c = -x_i y_i/r_i$
- $\partial d_i/\partial r = -1$

Solve the following over-determined system using any known numerical method, such as Cholesky Decomposition

$$\Delta = -[\mathbf{J}^T\mathbf{J} + \gamma\mathbf{I}]^{-1}\mathbf{J}^T\vec{\mathbf{d}} \tag{49}$$

where $\mathbf{I}$ is the identity matrix and $\gamma > 0$ is LM parameter. The best cylinder-fitting procedures are described in detail by Forbes and Shakarji [63,64].

6. Experimental results

In this section, an experimental comparison between ellipse-fitting methods is performed. Experiments were performed with synthetic and real data. The parameters involved in the comparison are

- Noise amplitude, represented by the standard deviation σ. We tested low, moderate, and high Gaussian noise distribution.
- Eccentricity e:

$$e = \sqrt{1 - \frac{b^2}{a^2}}, \quad 0 \le e \le 1 \tag{50}$$

The eccentricity represents how the shape of an ellipse varies from a circle ($e=0$) to a parabola ($e=1$).

- The elliptical arc position. Here, we vary the elliptic arc position to make it span areas of both low- and high-curvatures in the ellipse's contour.

1. *Synthetic data*: Synthetic ellipses were generated to simulate different combinations of noise, eccentricity, and arc curvature. The linear methods described in Section 4 were used to obtain the initial estimates. The estimated parameters were then improved using the LM method to find the best ellipse fit for the given data. The Goodness of Fit (GOF) was measured using Sum of Squared Residuals (SSR) and the number of

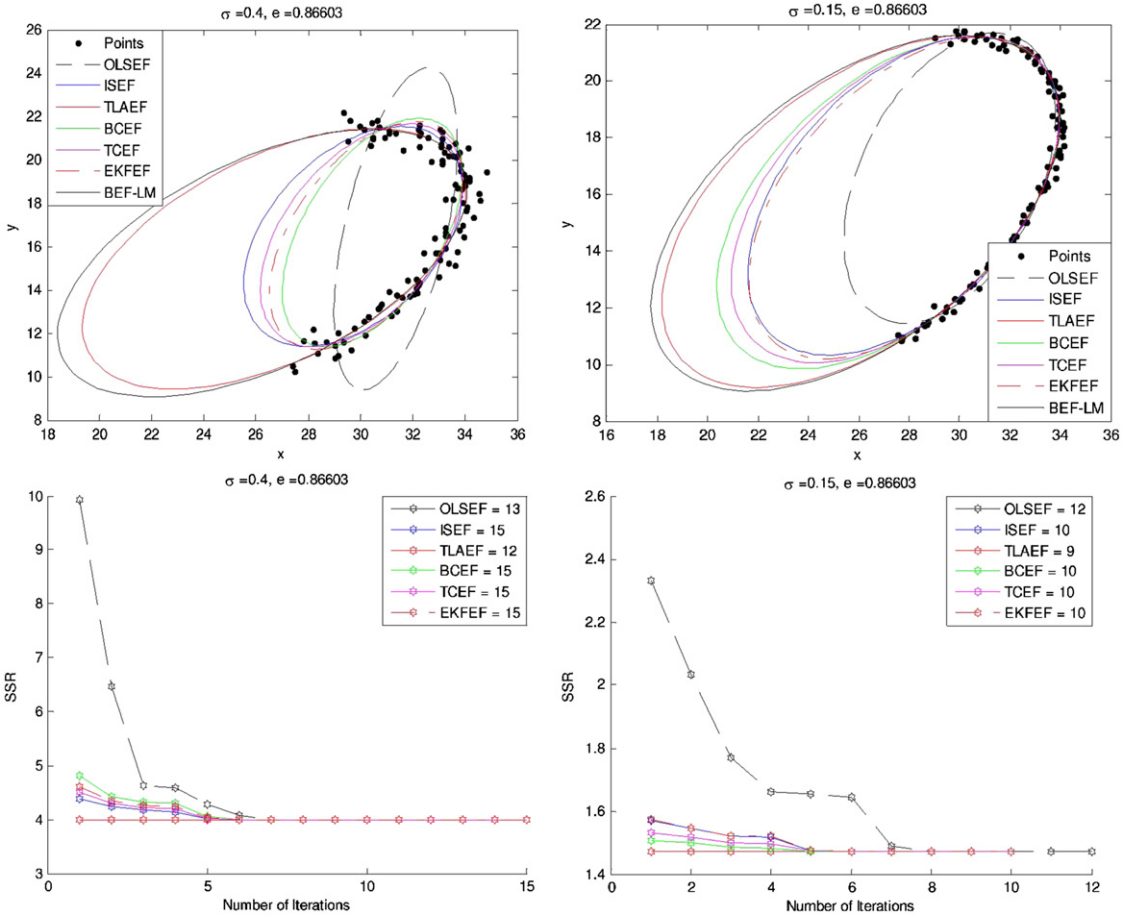

Fig. 12. Noise amplitudes (0.4 and 0.15), eccentricity (0.866), and both the low- and high-curvature arcs are sampled.

iterations required by the LM algorithm to converge.

The synthetic data were sampled from a transformed ellipse, with its parameters $\langle x_c, y_c, a, b, \phi \rangle$ set to $\langle 25, 15, 10, 5, \pi/6 \rangle$. The eccentricity was altered according to Eq. (50) by varying semi-minor axis b. A Gaussian noise was added, with an increasing amplitude of

- $\sigma = 0.05$ (low).
- $\sigma = 0.1$ (moderate).
- $\sigma = 0.15$ (high).
- $\sigma = 0.4$ (very high).

Data points were first sampled from a low-curvature arc, a high-curvature arc, and finally from an arc with both low- and high-curvatures. Some results of the experiments are presented in Figs. 4–13

2. *Measured data*: Three test objects were manufactured using a high accuracy rapid prototyping machine [65] (see Figs. 16, 18 and 21). The objects were scanned using the equipment described in Section 1. A single profile, which contained 2D data from each object, was used to fit an ellipse in order to

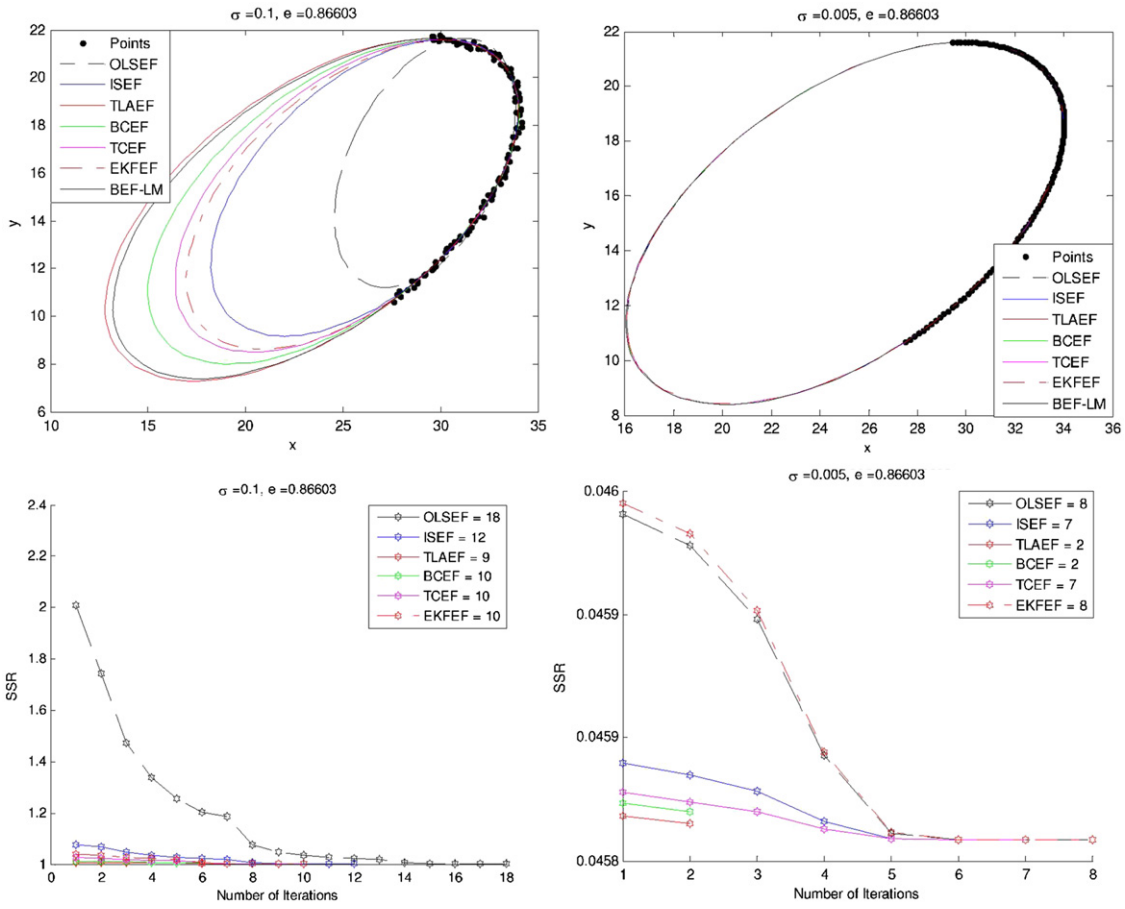

Fig. 13. Noise amplitudes (0.1 and 0.05), eccentricity (0.866), and both the low- and high-curvature arcs are sampled.

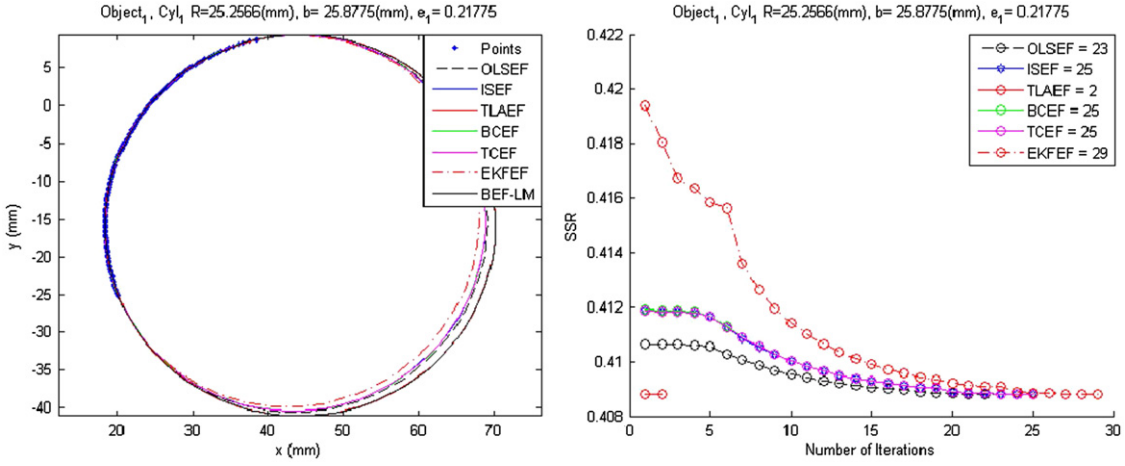

Fig. 14. Cylinder 1; Object 1.

estimate the radius of the corresponding cylinder (see Figs. 14, 15, 17, 19, and 20).

The exact radii of the cylinders were known, so the accuracy of the estimated cylinders' radii is presented in terms of absolute error in Table 1. In addition, Table 1 presents the deviation between the radii of cylinders estimated using ellipse fitting and the radii estimated using the cylinder fitting method. Table 2 shows the time of convergence for each method. The table shows significant differences between the ellipse fitting methods and the cylinder fitting method.

3D cylinders were fitted using the algorithm described in Section 5. See the reconstructed estimated models in Figs. 22–24. The algorithm was implemented using the parametric CAD system VARKON [66] developed by our research group [67].

We also performed comprehensive experiments to evaluate the stability and accuracy of the compared methods with regard to the radius estimation. In these tests we performed 50 estimations of the radii of cylinders with each of these methods. The cylinder surfaces were generated synthetically and corrupted with Gaussian noise of increasing amplitude, as in the first part. We assessed the stability and the accuracy by computing, respectively, the standard deviation and the Root Mean Square Error (RMSE) of the estimated radii. The performance of the ellipse fitting methods was assessed using synthetic and measured data. Results are shown in Tables 3 and 4. Figs. 25 and 26 compare their behavior with respect to the noise level.

7. Discussion

In this paper, we have compared several linear ellipse-fitting methods in order to find the most reliable linear method that can be implemented in our automatic 3D surface measuring system. The requirements that the ellipse fitting method should meet are

1. It should work with various ranges of noise amplitudes.
2. It should always fit an ellipse, even when a short elliptical arc is used.
3. It should provide a good initialization for the non-linear fitting technique.
4. It should work on high- and low-curvature arcs.
5. It should behave well with small and large eccentricity values.

Quantitatively, requirements 1, 4, and 5 mean that an ellipse-fitting method should not produce a degenerate ellipse for the allowed ranges of noise amplitude, eccentricity, and arcs. We assumed that the noise amplitude is less than 0.4, the eccentricity is always less than 0.96, and the arc length is above a quarter of the ellipse perimeter. Our laser scanning system allows us to obtain specific elliptic arcs that are within these ranges. Requirement 2 is verified by checking that the ellipse-fitting method does not produce another conic section, such as a hyperbola or a parabola, instead of an ellipse. Requirement 3 means that the ellipse estimate should be close to the global solution provided by the non-linear fitting; this requirement can be assessed by simply computing the number of iterations before convergence (convergence time). The performance versus the noise, the eccentricity and the arc's curvature is assessed by evaluating the accuracy of the estimated radii.

In addition, the selected method should be used to reliably estimate the initial parameters of a cylinder surface. These initial estimates can be employed to approximately localize the cylinder in the world coordinate system. This makes possible to generate a better scan path for the target cylinder surface, in which the laser profiles are perpendicular to the cylinder's axis.

By studying Figs. 4–13 and by comparing the results from Tables 1 and 2, we deduce the following behaviors for the linear methods:

- *OLSEF*: Performs well in terms of accuracy when the noise is low and the points are sampled from low-curvature part, or from both low- and high-curvature parts, of the ellipse. The method works on all sampled data, but it returns inaccurate

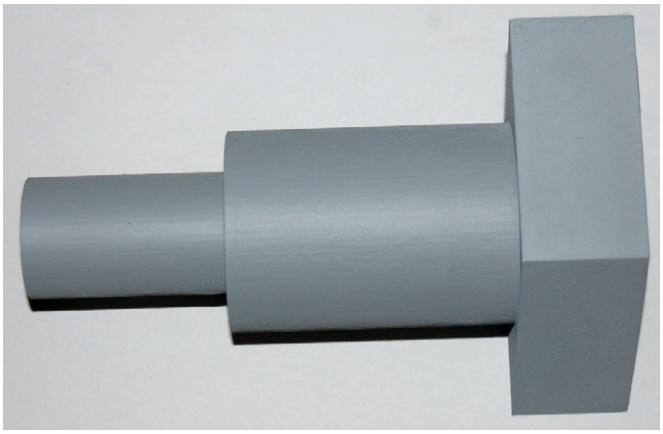

Fig. 16. Cylinders 1 and 2; Object 1.

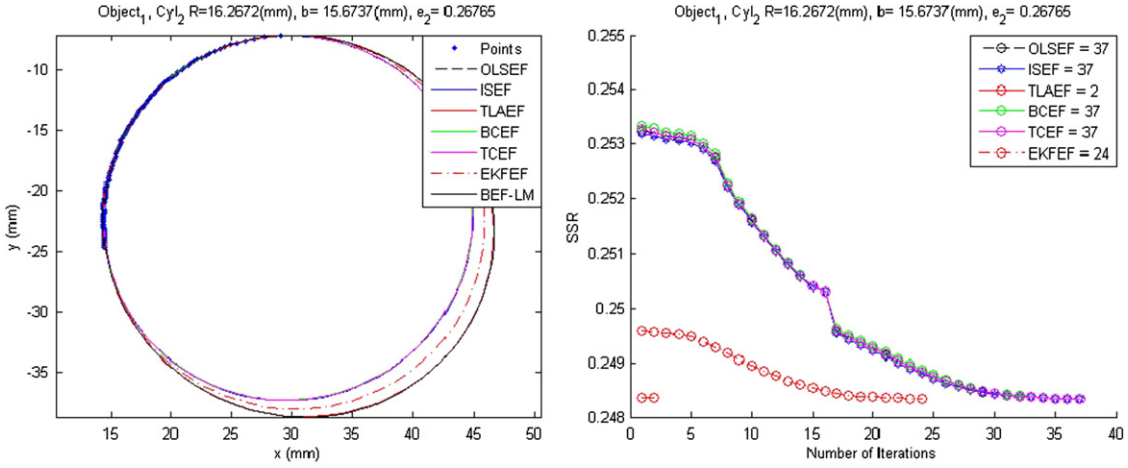

Fig. 15. Cylinder 2; Object 1.

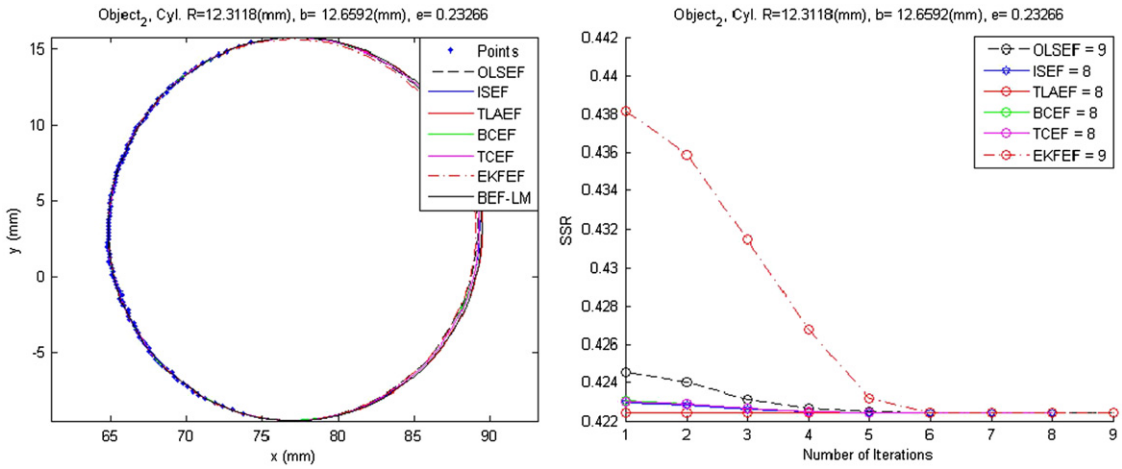

Fig. 17. Cylinder radius estimate; Object 2.

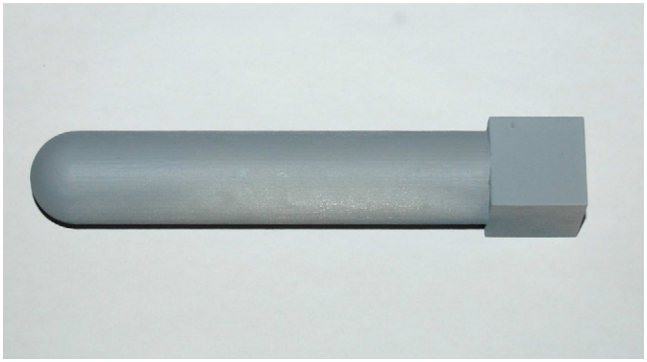

Fig. 18. Object 2.

ellipse as the noise amplitude and the eccentricity is increased. The method returns bad results in terms of accuracy and stability when an ellipse is fitted to sampled data with high noise, large eccentricity, and a high-curvature arc (see Figs. 10–13).

- *ISEF*: This method returns the best results in terms of accuracy and stability when high noise amplitude and large eccentricity are combined. The method always returns an ellipse. As the noise increases, the method performs well in comparison with other methods, as well as with the high-curvature arc sample data. This is due to the ellipse constraint being employed (see Figs. 10–13).
- *TLAEF*: This method is probably the best linear method, but it fails to fit an ellipse when noisy data are sampled from a high-curvature arc with large eccentricity (see Figs. 10 and 11). In this case the method returns a hyperbola instead of an ellipse.
- *BCEF*: This method fails to fit an ellipse to data sampled from a high-curvature arc when high-amplitude noise is combined with large eccentricity. The method is sensitive to the noise even if a high-curvature arc is sampled with low eccentricity, as it may return hyperbola or parabola (see Figs. 10 and 11). The method returns the best result when low-noise data is sampled from both the low- and high-curvature arcs and the eccentricity is moderate.
- *TCEF*: This method behaves like BCEF when a high-curvature arc and high amplitude noise is combined with large eccentricity, as can be seen in Figs. 10 and 11. It performs well in terms of accuracy and stability when moderate and low noise are combined with large eccentricity and sampled from a high-curvature arc.
- *EKFEF*: This method performs well in terms of accuracy and stability when low-noise data is sampled from a high-curvature arc and moderate eccentricity. The method works on all sampled data and does not fail with any sampled data, but it is an iterative linear method, which requires more computation.

Fig. 25 shows that EKFEF and TCEF achieve the best performance in terms of stability. At the other extreme is the BCEF, in which the behavior degrades significantly at high noise amplitude. At low and moderate noise amplitudes, the ISEF behaves similar to the EKFEF and TCEF, but the disparity becomes significant at high noise amplitudes. TLAEF is in the fourth rank and performs similar to the ISEF at a very high noise amplitude. The OLSEF behaves similar to the BCEF up to the third amplitude level, but performs consistently across all the noise amplitudes.

Fig. 26 shows the performance of the methods in terms of accuracy; roughly, it shows two groups. The first group includes ISEF, TCEF, TLAEF and EKFEF, while the second group is composed of BCEF and OLSEF. Methods in the first group clearly perform best and show nearly the same behavior. The second group exhibits more sensitivity to noise, as illustrated by the increasing disparity, with respect to the first group, as the noise amplitudes increases.

We summarized the above observations and investigations in Table 5. In general, all methods performed similarly in terms of accuracy and stability for long ellipse arcs and low noise levels. While the EKFEF exhibits the best performance in terms of stability and accuracy, it cannot be considered as the method of choice because of its non-compliance with the Fit ellipse criterion. Referring to Tables 3–5, respectively, we noticed that the TCEF and TLAEF methods were scoreless in terms of accuracy and stability and did not comply with the Fit ellipse criterion. The ISEF method was the only ellipse-specific method assuring a valid ellipse estimation (non-degenerate or resulting in another type of conic) and exhibiting a quite acceptable stability and accuracy. Indeed, its related standard deviation remains below 0.7 up to 0.1 noise amplitude, whereas its RMSE error is maintained below 0.6 across all the noise amplitude levels. Therefore, it is the method that leads to the best cylinder radius estimation when utilized for the initialization of the non-linear ellipse estimation technique. Based on the above comparative analysis of the different methods performances, we can conclude that the ISEF is the most reliable method for our application. However, this method has a disadvantage when dealing with noiseless data (i.e., when points are lying exactly on the ellipse). Here, the ISEF computation involves the inversion of an ill-conditioned matrix,

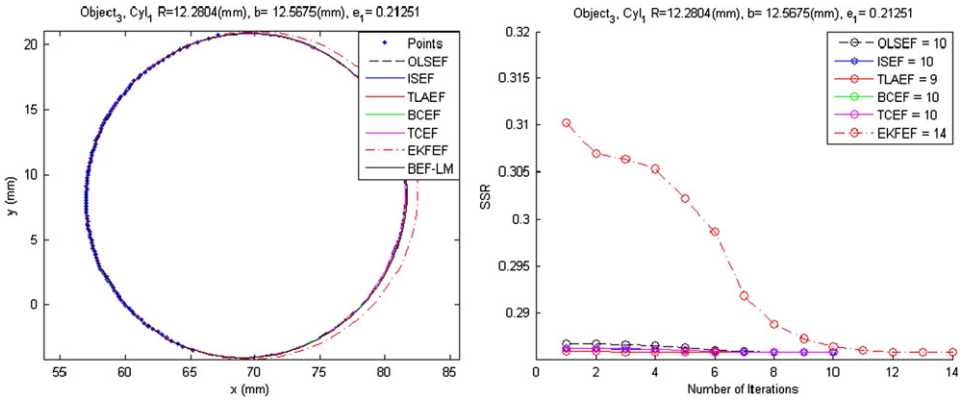

Fig. 19. Cylinder 1; Object 3.

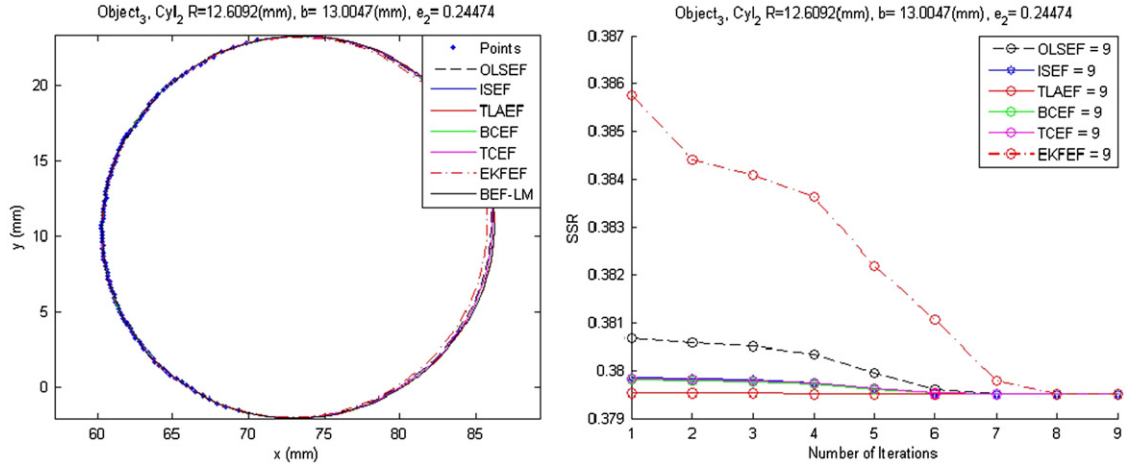

Fig. 20. Cylinder 2; Object 3.

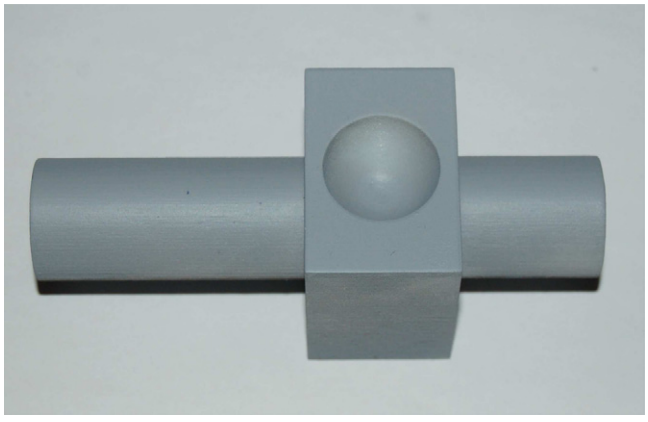

Fig. 21. Cylinders 1 and 2; Object 3.

which might cause an erroneous ellipse estimate (refer to [48,50]). Fortunately, having points exactly located on the actual ellipse is a scenario unlikely to happen in our application, as the data delivered by our scanning system is always noisy.

8. Conclusion and future work

In this paper we investigated the fitting of elliptical curves to 2D point data by testing and comparing several fitting algorithms, and then selected a combination of linear and non-linear methods that best suited the intrinsic properties of a laser profile scanner. We have considered the speed of computation, which is an important property for real-time industrial applications.

In addition, we considered the fact that we want a method that always fits an ellipse, even if the data consists only of a small portion of an ellipse section due to the actual shape of object or

Table 1
Estimated radii using ellipse fitting compared with the cylinder fitting and exact values.

Objects	Ellipse fitting (mm)		Cylinder fitting (mm)		Deviations (mm)		Errors (mm)	
	R_1	R_2	r_1	r_2	$\lvert\Delta_1\rvert$	$\lvert\Delta_2\rvert$	e_1	e_2
1	25.257	15.674	25.043	15.20	0.214	0.474	0.285	0.191
2	12.312	–	12.655	–	0.343	–	0.289	–
3	12.281	12.609	12.579	12.569	0.298	0.04	0.303	0.052

R_1 =Estimated radius of Cylinder 1 using ellipse fitting.
R_2 =Estimated radius of Cylinder 2 using ellipse fitting.
r_1 =Estimated radius of Cylinder 1 using cylinder fitting.
r_2 =Estimated radius of Cylinder 2 using cylinder fitting.
$|\Delta_1| = |R_1 - r_1|$.
$|\Delta_2| = |R_2 - r_2|$.
$e_1 = |R_1 - R_{1Exact}|$.
$e_2 = |R_2 - R_{2Exact}|$.

Table 2
Time-of-convergence of the 2D ellipse fitting methods compared with the 3D cylinder fitting method.

Methods	Object 1 (s)		Object 2 (s)	Object 3 (s)	
	t_{11}	t_{12}	t_{21}	t_{31}	t_{32}
ISEF	0.32	0.147	0.103	0.109	0.032
TLAEF	0.04	0.011	0.046	0.051	0.031
BCEF	0.285	0.144	0.064	0.071	0.031
TCEF	0.324	0.144	0.109	0.117	0.032
OLSEF	0.237	0.145	0.04	0.045	0.031
EKFEF	0.315	0.099	0.055	0.078	0.037
Cylinder fitting	2.579	0.455	12.173	0.559	0.526

t_{11}=Total processing time of Cylinder 1, Object 1.
t_{12}=Total processing time of Cylinder 2, Object 1.
t_{21}=Total processing time of Cylinder 1, Object 2.
t_{31}=Total processing time of Cylinder 1, Object 3.
t_{32}=Total processing time of Cylinder 2, Object 3.

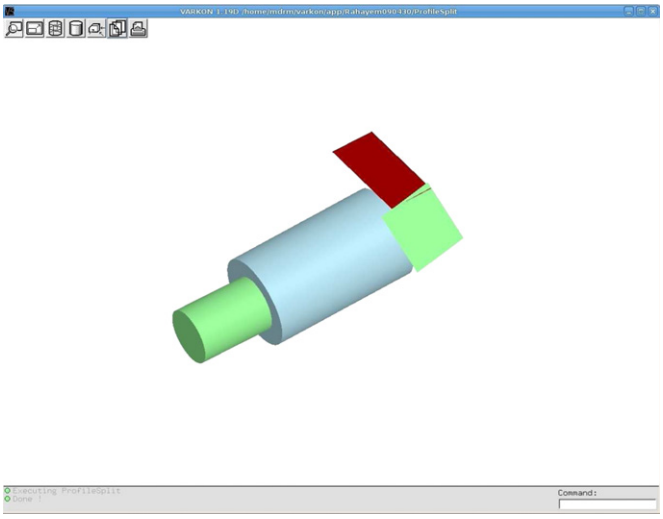

Fig. 22. Fitting cylinders to segmented surfaces – Object 1.

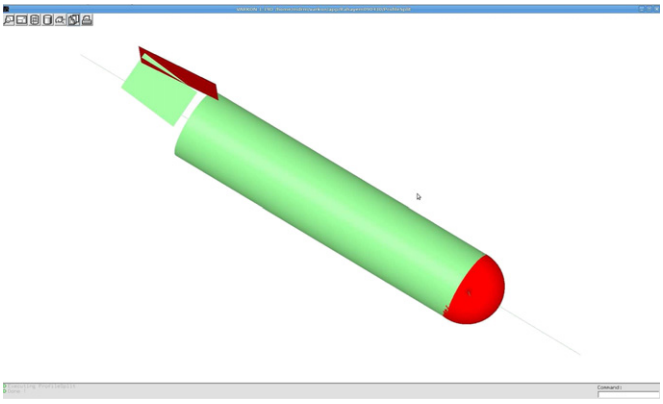

Fig. 23. Fitting cylinder to segmented surface – Object 2.

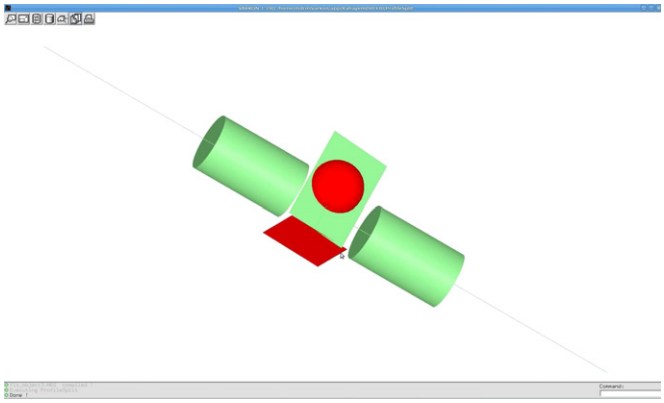

Fig. 24. Fitting cylinder to segmented surface – Object 3.

Table 3
Stability of ellipse fitting methods with various levels of noise.

σ	ISEF	TLAEF	BCEF	TCEF	OLSEF	EKFEF
0.05	0.16	0.79	2.22	0.163	2.12	0.16
0.1	0.70	1.87	2.50	0.311	2.44	0.31
0.15	1.40	2.47	2.84	0.493	2.54	0.49
0.4	2.89	3.15	11.54	1.353	2.97	1.21

Table 4
Accuracy of ellipse fitting methods with respect to the increasing noise level.

σ	ISEF	TLAEF	BCEF	TCEF	OLSEF	EKFEF
0.05	0.05	0.08	0.223	0.05	0.21	0.05
0.1	0.17	0.12	0.40	0.09	0.45	0.09
0.15	0.26	0.33	0.67	0.15	0.55	0.15
0.4	0.59	0.81	2.40	0.64	1.85	0.72

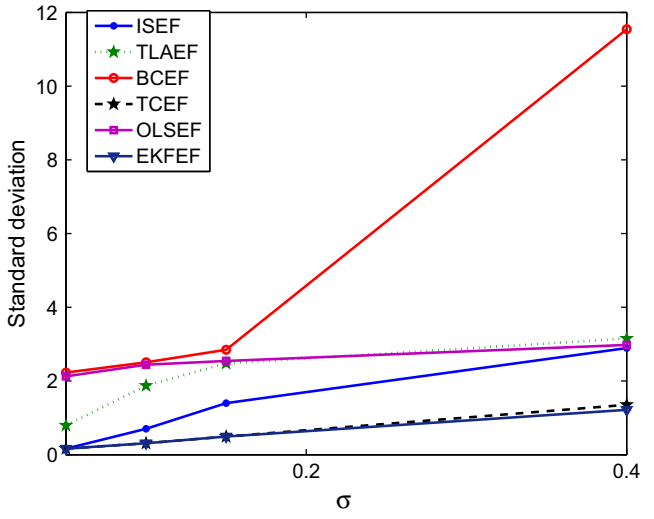

Fig. 25. Stability performance of the ellipse fitting methods with respect to the noise level.

the occlusion of the scanner. Finally, we presented a new method for cylindrical surface reconstruction that combines a direct solution, based on the elliptic arc profiles, and a robust non-linear optimization technique in which the elliptical arc fitting is used to evaluate the initial estimates for the cylinder-fitting algorithm.

We scanned three different objects with cylindrical shapes and showed that all cylindrical surfaces have been correctly identified with high accuracy. Usually, cylindrical surface-fitting methods operate on 3D point clouds, but the new method presented here takes into account the properties of a 2D laser profile scanner and uses these to increase the speed of computation through data reduction. The data reduction is discussed in Section 5, where cylinder's parameters are obtained by performing an ellipse fitting. The presented method could be used, for example, to plan new optimal scan paths for scanning a cylinder located on the turntable. The new scan path will then be used to achieve new

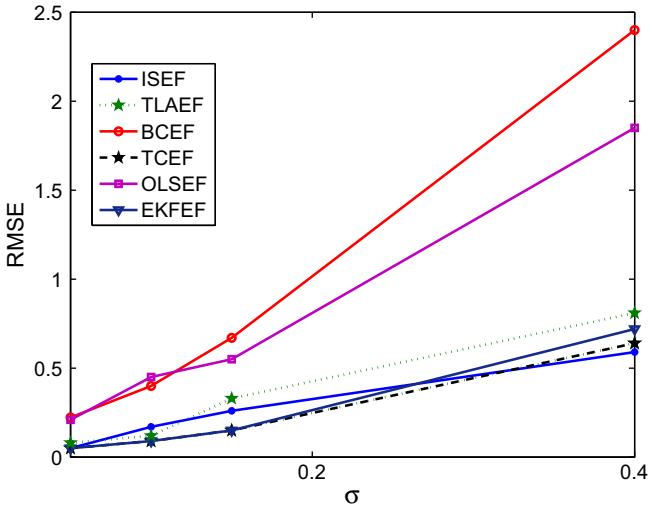

Fig. 26. Accuracy performance of the ellipse fitting methods with respect to the noise level.

Table 5
Behavior of ellipse fitting methods.

Criterion	ISEF	TLAEF	BCEF	TCEF	OLSEF	EKFEF
High noise	***	*	*	*	*	**
Fit ellipse	***	*	**	**	**	**
Non-linear convergence	***	**	**	**	*	**
High curvature	***	**	*	*	*	**
High eccentricity	***	**	*	**	*	**
Stability	**	**	*	***	**	***
Accuracy	**	**	*	**	*	**

*: Low; **: Fair; ***: Good.

profiles with better a scan depth and a projected angle (see [68,69]).

Acknowledgments

We would like to thank the authors of [34], who made their code available on the Internet. Also, we would like to thank Dr. Pál Ledneczki, Budapest University of Technology and Economics, for a discussion on descriptive geometry and for preparing the figure in Section 5. The project is supported by the Modeling and Simulation Research Center (MoS) at Campus Alfred Nobel, Örebro University, in Sweden. Finally, we would like to thank the anonymous reviewers for their constructive comments.

References

[1] Larsson S, Kjellander J. An industrial robot and a laser scanner as a flexible solution towards an automatic system for reverse engineering of unknown objects. In: Proceedings of ESDA04—seventh biannual conference on engineering systems design and analysis; 2004. p. 341–50.
[2] Larsson S, Kjellander J. Motion control and data capturing for laser scanning with an industrial robot. Robot Autonomous Syst 2006;54(6):453–60.
[3] Larsson S, Kjellander J. Path planning for laser scanning with an industrial robot. Robot Autonomous Syst 2008;56(7):615–24.
[4] Kjellander J, Rahayem M. An integrated platform for 3d measurement with geometric reverse engineering. Comput-Aided Des Appl 2009;6(6):877–87.
[5] Rahayem M, Kjellander J. Quadric segmentation and fitting of data captured by a laser profile scanner mounted on an industrial robot. Int J Adv Manuf Technol 2011;52(1–4):155–69.
[6] Blais F. Review of 20 years of range sensor development. J Electron Imaging 2004;13(1):231–43.
[7] Pito R, Bajcsy R. Solution to the next best view problem for automated cad model acquisition of free-form objects using range cameras. In: Proceedings of the SPIE symposium on intelligent systems and advanced manufacturing; 1995. p. 78–89.
[8] Chan VH, Bradley C, Vickers G. A multi-sensor approach for rapid digitization and data segmentation in reverse engineering. J Manuf Sci Eng 2000;122(4):725–33.
[9] Milroy MJ, Bradley C, Vickers G. Automated laser scanning based on orthogonal cross sections. Mach Vis Appl 1969;9(3):106–18.
[10] Feng H-Y, Liu Y, Xi F. Analysis of digitizing errors of a laser scanning system. Precis Eng 2001;25(3):185–91.
[11] Xi F, Liu Y, Feng H-Y. Error compensation for three-dimensional line laser scanning data. Int J Adv Manuf Technol 2001;18(3):211–6.
[12] Lee KH, Park H, Son S. A framework for laser scan planning of freeform surfaces. Int J Adv Manuf Technol 2001;17(3):171–80.
[13] Lee KH, Park H. Automated inspection planning of free-form shape parts by laser scanning. Robot Comput-Integr Manuf 2000;16(4):201–10.
[14] Son S, Park H, Lee KH. Automated laser scanning system for reverse engineering and inspection. Int J Mach Tools Manuf 2002;42:889–97.
[15] Son S, Kim S, Lee K. Path planning of multi-patched freeform surfaces for laser scanning. Int J Adv Manuf Technol 2003;22(5–6):424–35.
[16] Xie Z, Zhang Z, Jin M. Development of a multi-view laser scanning sensor for reverse engineering. Meas Sci Technol 2006;17(8):2319–27.
[17] Robertson C, Fisher R. Shape recovery and analysis of large screw threads. In: Proceedings of the third international conference on 3-D digital imaging and modeling; 2001. p. 300–5.
[18] Callieri M, Fasano A, Impoco G, Cignoni P, Scopigno R, Parrini G, et al. Roboscan: an automatic system for accurate and unattended 3D scanning. In: IEEE proceedings of the second symposium on 3D data processing, visualization, and transmission; 2004. p. 805–12.
[19] Scott WR, Roth G, Rivest J-F. View planning for automated three-dimensional object reconstruction and inspection. ACM Comput Surv 2003;35(1):64–96.
[20] Hayes MJD, Leitner M, O'Leary P, Ofner R, Sallinger C. An integrated optical-robotics measurement system. In: Proceedings of the 18th Canadian congress of applied mechanics (CANCAM 2001), St. John's, NL, Canada; 2001. p. 287–8.
[21] Reindl I, O'Leary P. Instrumentation and measurement method for the inspection of peeled steel rods. In: Proceedings of IEEE instrumentation and measurement technology conference; 2007. p. 1–6.
[22] O'Leary P, Schalk P, Ofner R. Instrumentation and analysis-methods for the measurement of profiles using light sectioning. In: Proceedings of the IEEE instrumentation and measurement technology conference; 2006. p. 1108–13.
[23] Schalk P, O'Leary P. Measuring and analyzing cross-sectional profiles of rotating objects using light sectioning. IEEE Trans Instrum Meas 2008;57(10):2329–38.
[24] Bradley BD, Chan ADC, Hayes MJD. A 3D scanning system for biomedical purposes. Int J Adv Media Commun 2009;3(1–2):35–54.
[25] Bradley BD, Chan ADC, Hayes MJD. A simple, low cost, 3D scanning system using the laser light-sectioning method. In: Proceedings of instrumentation and measurement technology conference; 2008. p. 299–304.
[26] Reinhart G, Tekouo W. Automatic programming of robot-mounted 3d optical scanning devices to easily measure parts in high-variant assembly. CIRP Ann – Manuf Technol 2009;58(1):25–8.
[27] Van Gestel N, Cuypers S, Bleys P, Kruth J-P. A performance evaluation test for laser line scanners on CMMs. Opt Lasers Eng 2009;47(3–4):336–42.
[28] D'Apuzzo N. Overview of 3d surface digitization technologies in Europe. In: Proceedings of three-dimensional image capture and applications VII. Society of photo-optical instrumentation engineers (SPIE), vol. 6056; 2006. pp. 42–54.
[29] Yuen HK, Illingworth J, Kittler J. Detecting partially occluded ellipses using the Hough transform. Image Vis Comput 1989;7(1):31–7.
[30] Wei L, Jinglu T. Detection of incomplete ellipse in images with strong noise by iterative randomized Hough transform (IRHT). Pattern Recognit 2008;41(4):1268–79.
[31] Leavers VFF. Shape detection in computer vision using the Hough transform. Secaucus, NJ, USA: Springer-Verlag, New York, Inc.; 1992.
[32] Han F, Guo Y, Wang L. A new ellipse detector based on Hough transform. In: Proceedings of second international conference on information and computing science; 2009. p. 301–5.
[33] Chia AYS, Leung MKH, How-Lung E, Rahardja S. Ellipse detection with Hough transform in one dimensional parametric space. In: Proceedings of IEEE international conference on image processing; 2007. p. 333–6.
[34] Gander W, Golub G, Strebel R. Least-squares fitting of circles and ellipses. In: Bulletin of the Belgian mathematical society – numerical analysis – a numerical analysis conference in honour of Jean Meinguet, 1996. p. 63–84.
[35] Bookstein F. Fitting conic sections to scattered data. Comput Graph Image Process 1979;9(1):56–71.
[36] Zheng Z. Parameter estimation techniques: a tutorial with application to conic fitting. Image Vis Comput 1997;15(1):59–76.
[37] Jianfei M, Rong X, Weilong D. A compound and robust algorithm for ellipse detection. In: Proceedings of the 16th international conference on artificial reality and telexistence—workshops; 2006. p. 381–6.
[38] Wan W, Ventura JA. Segmentation of planar curves into straight-line segments and elliptical arcs. Graphical Models Image Process 1997;59(6):484–94.
[39] O'Leary P, Zsombor-Murray P. Direct type-specific least-square fitting of hyperbolae and ellipse. J Electron Imaging 2004;13(3):492–503.
[40] O'Leary P, Harker M, Zsombor-Murray P. Direct and least square fitting of coupled geometric objects for metric vision. In: IEE proceedings of vision, image and signal processing; 2005. p. 687–94.

[41] Taubin G. Estimation of planar curves, surfaces, and non planar space curves defined by implicit equations with applications to edge and range image segmentation. IEEE Trans Pattern Anal Mach Intell 1991;13(11):1115–38.
[42] Harker M, O'Leary P, Zsombor-Murray P. Direct type-specific conic fitting and eigenvalue bias correction. Image Vis Comput 2008;26(3):372–81.
[43] Hahn K, Jung S, Han Y, Hahn H. A new algorithm for ellipse detection by curve segments. Pattern Recognit Lett 2008;29(13):1836–41.
[44] Fitzgibbon A, Pilu M, Fisher RB. Direct least square fitting of ellipses. IEEE Trans Pattern Anal Mach Intell 2009;21(5):476–80.
[45] Wu J. Robust real-time ellipse detection by direct least-square-fitting. In: Proceedings of international conference on computer science and software engineering; 2008. p. 923–7.
[46] Halir R, Flusser J. Numerically stable direct least squares fitting of ellipses. In: Proceedings of WSCG '98 – sixth international conference in central Europe on computer graphics and visualization; 1998. p. 125–32.
[47] Nguyen TM, Ahuja S, Wu Q. A real-time ellipse detection based on edge grouping. In: Proceedings of IEEE international conference on systems, man and cybernetics; 2009. p. 3280–6.
[48] Maini ES. Enhanced direct least square fitting of ellipses. Int J Pattern Recognit 2006;20(6):939–54.
[49] Schleicher DCH, Zagar BG. Image processing to estimate the ellipticity of steel coils using a concentric ellipse fitting algorithm. In: Proceedings of the ninth international conference on signal processing; 2008. p. 884–90.
[50] Greggio N, Bernardino A, Laschi C, Dario P, Santos-Victor J. An algorithm for the least square-fitting of ellipses. In: 22nd IEEE international conference on tools with artificial intelligence (ICTAI); 2010. p. 351–3.
[51] Barwick DS. Very fast best-fit circular and elliptical boundaries by chord data. IEEE Trans Pattern Anal Mach Intell 2009;31(6):1147–52.
[52] Ellis T, Abbood A, Brillault B. Ellipse detection and matching with uncertainty. Image Vis Comput 1992;10(5):271–6.
[53] Rosin P. A note on the least squares fitting of ellipses. Pattern Recognit Lett 1993;14(10):799–808.
[54] Porrill J. Fitting ellipses and predicting confidence envelopes using a bias corrected Kalman filter. Image Vis Comput 1990;8(1):37–41.
[55] Werghi N, Doignon C, Abba G. Ellipse fitting and three-dimensional localization of objects based on elliptic features. In: Proceedings of the international conference on image processing; 1996. p. 57–60.
[56] Ahn SJ, Rauh W, Warnecke H-J. Least-squares orthogonal distances fitting of circle, sphere, ellipse, hyperbola, and parabola. Pattern Recognit 2001;34(12):2283–303.
[57] Ahn SJ. Least squares orthogonal distance fitting of curves and surfaces in space. Springer; 2004.
[58] Faber P, Fisher R. Estimation of general curves and surfaces to edge and range data by Euclidean fitting. Technical Report, University of Edinburgh – Division of Informatics, EDI-INF-RR-0146; 2002.
[59] Gander W, Hrebicek J. Solving problems in scientific computing using MAPLE and MATLAB. Springer; 1993.
[60] MATLAB. 〈http://www.mathworks.com〉.
[61] Rahayem M. Segmentation and fitting for geometric reverse engineering-processing data captured by a laser profile scanner mounted on an industrial robot. PhD thesis, Örebro University; 2010.
[62] Werghi N, Fisher R, Robertson C, Ashbrook A. Object reconstruction by incorporating geometric constraints in reverse engineering. Comput-Aided Des 1999;31:363–99.
[63] Forbes A. Least-squares best-fit geometric elements. Technical Report, National Physical Laboratory, NPL Report DITC 140/89; 1991. Revised edition – February 1991. ISSN 0262-5369.
[64] Shakarji CM. Least-squares fitting algorithms of the NIST algorithm testing system. J Res Natl Inst Stand Technol 1998;633-41.
[65] Objet Geometries Ltd. 〈http://www.objet.com/3D-Printer/Eden250〉.
[66] Varkon CAD Tool. 〈http://varkon.sourceforge.net〉.
[67] CAD Technology Research Group. 〈http://www.oru.se/nt/cad〉.
[68] Rahayem M, Kjellander J, Larsson S. Accuracy analysis of a 3d measurement system based on a laser profile scanner mounted on an industrial robot with a turntable. In: Proceedings of ETFA'07 IEEE conference on emerging technologies and factory automation; 2007. p. 880–3.
[69] Rahayem M, Kjellander J, Larsson S. Geometric reverse engineering using a laser profile scanner mounted on an industrial robot. In: Proceedings of the sixth international conference of DAAAM Baltic industrial engineering; 2008. p. 147–52.